RGNZ/MGPB

Facies Architecture and Sedimentary Provenance of the Miocene Ombilin Formation: Interplay of Tectonics and Eustasy in a Neogene Intermontane Basin, Central Sumatra, Indonesia

Rudarsko-geološko-naftni zbornik
(The Mining-Geology-Petroleum Engineering Bulletin)
DOI: 10.17794/rgn.2026.2.5

Original scientific paper

Aurio Erdi[1]*, Syahreza S. Angkasa[2], Eko Suwarno[2], Aswan[3]
[1] *Research Centre for Geological Resources, National Research and Innovation Agency (BRIN), Indonesia.*
[2] *Directorate of Geothermal, Ministry of Energy and Mineral Resources, Indonesia.*
[3] *Geological Engineering, Faculty of Earth Science and Technology (FITB), Institut Teknologi Bandung, Indonesia.*

Abstract
The Early–Middle Miocene Ombilin Formation in the intermontane Ombilin Basin, Central Sumatra, records a critical interval of paleoenvironmental change shaped by regional tectonics and global sea-level fluctuations. Despite its significance, the formation's sedimentological architecture, provenance, and sea-level history have been poorly constrained. This study integrates detailed outcrop-based sedimentary logging and petrographic analysis to address these gaps. Ten lithofacies are identified and grouped into three facies associations: open marine, tidal-influenced channels, and intertidal mixed tidal flats deposits. Their vertical distributions show normal and inverse transitions. The normal transition indicates a shift from sublittoral to tidally dominated environments, interpreted as a result of seaward progradation driven by increased sediment supply from the uplifting Barisan Mountains and short-term global sea-level falls (e.g. SEA34–SEA46). The inverse transition, however, indicates a transgression occurred in the Ombilin Basin. Petrographic analysis in the Ombilin Formation show arkosic sandstones sourced primarily from a magmatic arc, consistent with contemporaneous volcanism west of the basin, with minor reworking of marine units and older clastic materials. Stratigraphic evidence suggests an initial regression, likely driven by the uplifting of Barisan Mountain and global sea-level fall, which occurred in the Ombilin Basin during Early Miocene. This event was followed by deposition aligned with global transgressive trends. These findings provide new insight into the sedimentary evolution, provenance, and tecto-no-eustatic interplay controlling Ombilin Basin development during the Early–Middle Miocene.

Keywords:
tidal-related deposits, Sinamar sub-basin, sedimentology, provenance, tectonics

1. Introduction

The Ombilin Basin has been classified as one of the intermontane basins (**Koesoemadinata, 2020**) within the Barisan Mountain Range in Central Sumatra, Indonesia (**e.g. Koesoemadinata and Matasak, 1981; Habrianta et al., 2018**). Owing to this unique tectonic location, the basin has been infilled with a substantial thickness of Cenozoic sediments, which has been interpreted as a response to the region's dynamic tectonic setting, particularly its proximity to the active Sumatra Fault System and the Barisan Mountains (**Figure 1a,b; e.g. Howells, 1997; Barber et al., 2005**). Among the sedimentary successions, the Ombilin Formation has been highlighted as a crucial stratigraphic unit for interpreting the paleoenvironmental history of the basin during a phase characterized by regional transgression, the occurrence of the Barisan being uplifted (**e.g. Koesoemadinata and Matasak, 1981; Koning, 1985**), and/or a transition from a eustatic sea-level fall to a rise in the Early Miocene (**e.g. Zaim et al., 2012; Morley et al., 2021**).

Despite the recognized significance of the Ombilin Formation in recording tectonic activity and sea-level fluctuations, limited understanding has been established regarding its sedimentological characteristics, provenance, depositional environment, and their linkage to global eustatic changes. The formation has generally been interpreted as an Early Miocene marine deposit, distinguished by grey calcareous shales, clays, and locally developed bioclastic limestone layers, which have been associated with a transitional to neritic depositional environment (**e.g. Koesoemadinata and Matasak, 1981; Barber et al., 2005; Linggadipura et al., 2018**). This previous interpretation of the depositional environment was supported by a limited analysis of lithofacies variability, sedimentary structures, and fossils, constraining reconstructions of the paleoenvironments that prevailed during its formation. These previous studies, however, have not clearly defined the impact of the glob-

* Corresponding author: Aurio Erdi
e-mail address: auri002@brin.go.id
Received: 22 May 2025. Accepted: 2 October 2025.
Available online: 13 March 2026

al transition from eustatic fall to rise on the sedimentary dynamics of the Ombilin Formation during the Early Miocene age. Such a relationship is considered critical for a comprehensive paleoenvironmental reconstruction of the basin during this period. Moreover, provenance studies specifically addressing the Early Miocene Ombilin Formation have remained scarce (**Adhiperdana, 2010; Yeni, 2011**). The origin of the clastic material is regarded as a key element in deciphering the tectonic development of the basin and its relation to the adjacent geological domains during the Early Miocene.

In this study, the existing gaps in understanding the Ombilin Formation have been addressed through an integrated sedimentological and petrographic investigation conducted in the area adjacent to the Tanjung Ampalu Fault, situated within the Sinamar sub-basin of the Ombilin Basin. To achieve this, several research questions have been posed: (1) how can the lateral and vertical variability of facies and depositional environments within the Ombilin Formation be characterized?; (2) what does the provenance of the formation reveal about sediment sources?; and, (3) how are facies architecture and provenance related to regional tectonics in Sumatra and broader Miocene eustatic trends across Southeast Asia? Through the examination of sediment textural and compositional characteristics, new insight into the depositional processes and environmental conditions that governed the formation's development has been obtained. The provenance and potential sediment dispersal pathways into the basin have been inferred through petrographic analysis of framework grains. Ultimately, the integration of these findings has been employed to reconstruct the paleoenvironmental evolutions of the Ombilin Basin during the Early Miocene and to evaluate its linkage with regional tectonic activity in Sumatra and contemporaneous eustatic sea-level fluctuations across Southeast Asia.

2. Geological Settings

The study area is situated within the Ombilin Basin, a Cenozoic intermontane basin covering approximately 25 × 60 km² and aligned parallel to the NW–SE structural trend of Sumatra (**Figure 1; e.g. Koesoemadinata and Matasak, 1981; Anastasia et al., 2012; Habrianta et al., 2018**). This basin is located within the Bukit Barisan Mountain range, on the continental crust where the magmatic arc and the Sumatra Fault Zone (SFZ) are also present (**e.g. Van Bemmelen, 1949; Situmorang et al., 1991; Noeradi et al., 2005; Zaim et al., 2012**). The eastern margin of the basin is bounded by the Takung Fault, whereas its western and southern flanks are bordered by pre-Cenozoic lithologies composed of limestone, metamorphic, and granitic complexes, as well as by the NW-trending Barisan Fault System (**Figure 1b; e.g. Koesoemadinata and Matasak, 1981; Koning, 1985; Noeradi et al., 2005**). Toward the northwest, the basin is observed to transition into either the basement ridge of the Tungkar High or the active volcanic centers of Marapi and Malintang (**Koning, 1985**). Furthermore, the basin is transected centrally by N–S trending Tanjung Ampalu Fault, subdividing it into the Paleogene-aged Talawi sub-basin in the west and the Neogene-aged Sinamar sub-basin in the east (**Figure 1b; e.g. Koning, 1985; Situmorang et al., 1991; Barber et al., 2005**).

The Ombilin Basin has been filled with up to 4600 m of Eocene to Middle Miocene deposits, which overlie the pre-rift Pre-Cenozoic basement (**e.g. Koning, 1985; Whateley and Jordan, 1989**). The pre-Cenozoic basement units are exposed along the basin margins, represented by Permian to Upper Cretaceous granites, Middle to Late Triassic limestones, and Permo-Carboniferous limestones, and considered part of the Mergui and Woyla accretionary terrains (**e.g. Fletcher and Yarmanto, 1993; Noeradi et al., 2005**). The Eocene to Middle Miocene deposits, however, are believed to have been eroded for approximately 3600 meters in the western side of the basin (**Whateley and Jordan, 1989**). The Eocene to Middle Miocene deposits reflect tectonostratigraphic stages in the Ombilin Basin (see **Figure 2**).

The initial period of Ombilin Basin filling was reflected by the deposition of early syn-rift formations, unconformably overlying the Pre-Cenozoic Basement (**Figures 1b, d and 2; Koning, 1985; Fletcher and Yarmanto, 1993**). The early syn-rift formations consist of interfingering deposits of the alluvial fans, and the lake and lacustrine deposits of the Brani and Sangkarewang formation, respectively (**e.g. Whateley and Jordan, 1989; Koesoemadinata and Matasak, 1981**). Debates regarding age determination of these formations have arisen, with proposed ages ranging from Paleocene (**Koesoemadinata and Matasak, 1981; Whateley and Jordan, 1989**), Paleocene to Early Eocene (**Noeradi et al., 2005**), Eocene (**e.g. Fletcher and Yarmanto, 1993; Situmorang et al., 1991; Murray, 2020**), or Eocene to Oligocene (**Barber et al., 2005**). These formations were deposited during the formation of the graben (**Van Bemmelen, 1947; Barber et al., 2005**) and are associated with: (i) Middle Cretaceous to Early Cenozoic orogenesis (**e.g. Katili and Hehuwat, 1967; Koesoemadinata and Matasak, 1981**); (ii) the nucleation of the en-echelon array of the Sumatra Fault Zone (SFZ; **Koning, 1985; Situmorang et al., 1991**); or (iii) the extensional rifting of back-arc settings in response to subduction (**e.g. Fletcher and Yarmanto, 1993; Noeradi et al., 2005**).

The late syn-rift formation was deposited either unconformably (**Barber et al., 2005**) or conformably (**Koesoemadinata and Matasak, 1981; Noeradi et al., 2005**) above the early syn-rift formations and is represented by the fluvio-deltaic deposits of the Sawahlunto Formation (see **Figures 1b-d** and **2**). This formation is characterized by fining-upward sequences of interbedded fine to medium sandstones, shales, and coals (**What-**

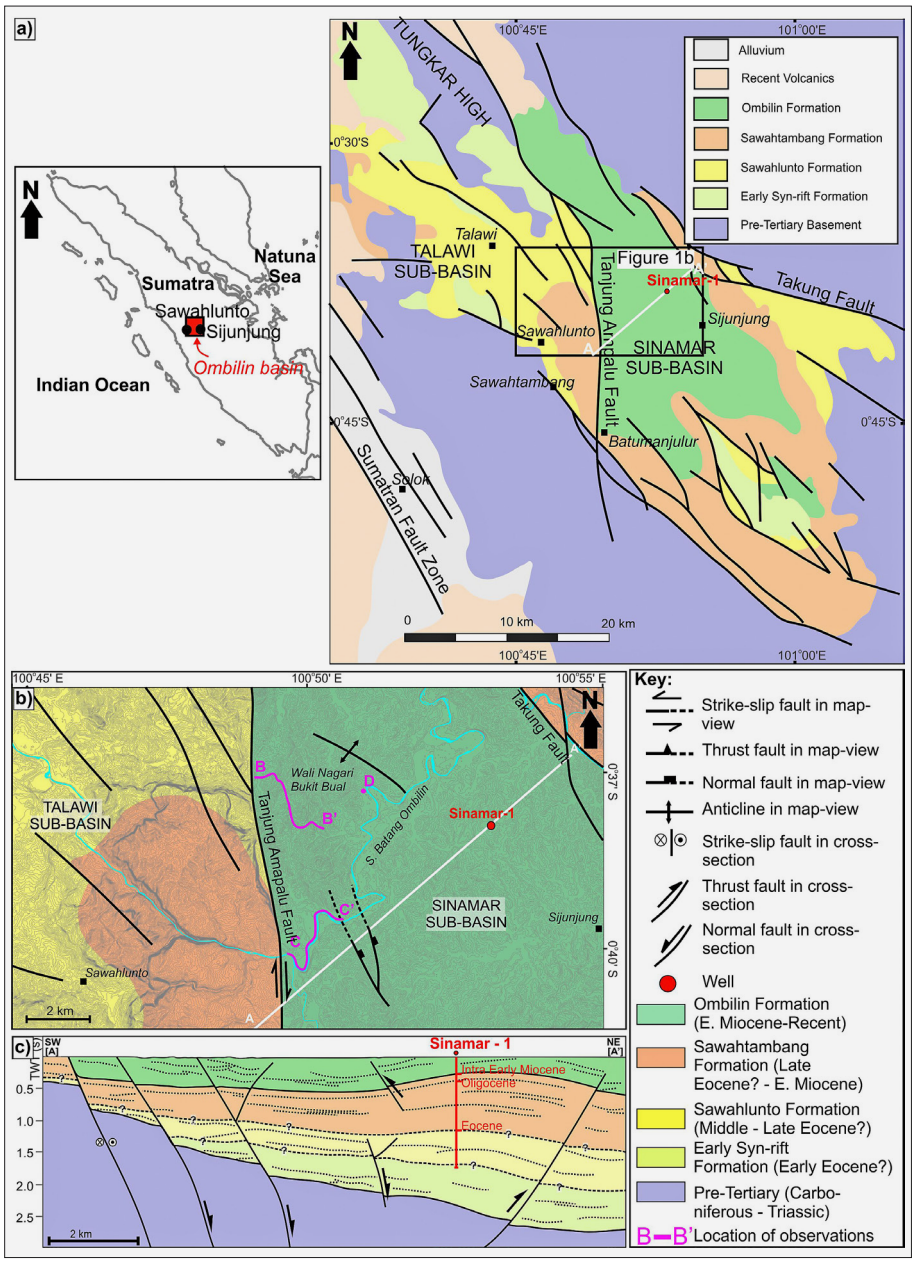

Figure 1. a) Regional map of Sumatra, showing the location of the Ombilin Basin. b) Simplified geological map of the study area in the Ombilin Basin (compiled from **Barber et al, 2005**; **Zaim et al., 2012**). c) Structural cross-sections across the study area (**Putra et al., 2021**).

eley and Jordan, 1989; Fletcher and Yarmanto, 1993), which transition upward into thick-bedded sandstones and shales (**Koesoemadinata and Matasak, 1981**), and laterally into glauconitic conglomeratic sandstones (**Noeradi et al., 2005**). Deposition of this formation has been interpreted to have occurred in meandering fluvial to deltaic environments (**Koesoemadinata and Matasak, 1981; Noeradi et al., 2005**), with the age variously assigned from the Eocene (**Koesoemadinata and Matasak, 1981; Whateley and Jordan, 1989**; **Murray, 2020**) to Oligocene–Early Miocene (**Bartram and Nugrahaningsih, 1990; Situmorang et al., 1991; Fletcher and Yarmanto, 1993; Noeradi et al., 2005**).

The late stage of basin infill in the Ombilin Basin has been marked by the deposition of post-rift successions. During the early post-rift phase, the Sawahtambang Formation was deposited either conformably (**Koesoemadinata and Matasak, 1981**) or unconformably (**Koning, 1985; Whateley and Jordan, 1989**) above the Sawahlunto Formation (see **Figures 1b-d** and **2**). The Sawahtambang Formation is characterized by thick, channelled and cross-bedded quartzose to feldspathic sandstones and conglomerates, transitioning upward into fine-grained sandstones, mudrocks, thin coal beds, and interbedded tuffs (**e.g. Noeradi et al., 2005; Barber et al., 2005**). This formation is interpreted to have been deposited within a fluvial-dominated environment (**Koesoemadinata and Matasak, 1981; Howells, 1997**). This event occurred between the Eocene to Early Miocene (**e.g. Koning et al., 1985; Noeradi et al., 2005**), when back-arc subsidence, magmatic arc activation, and strike-slip deformation along the Sumatra Fault System occurred (**Howells, 1997; Barber et al., 2005**).

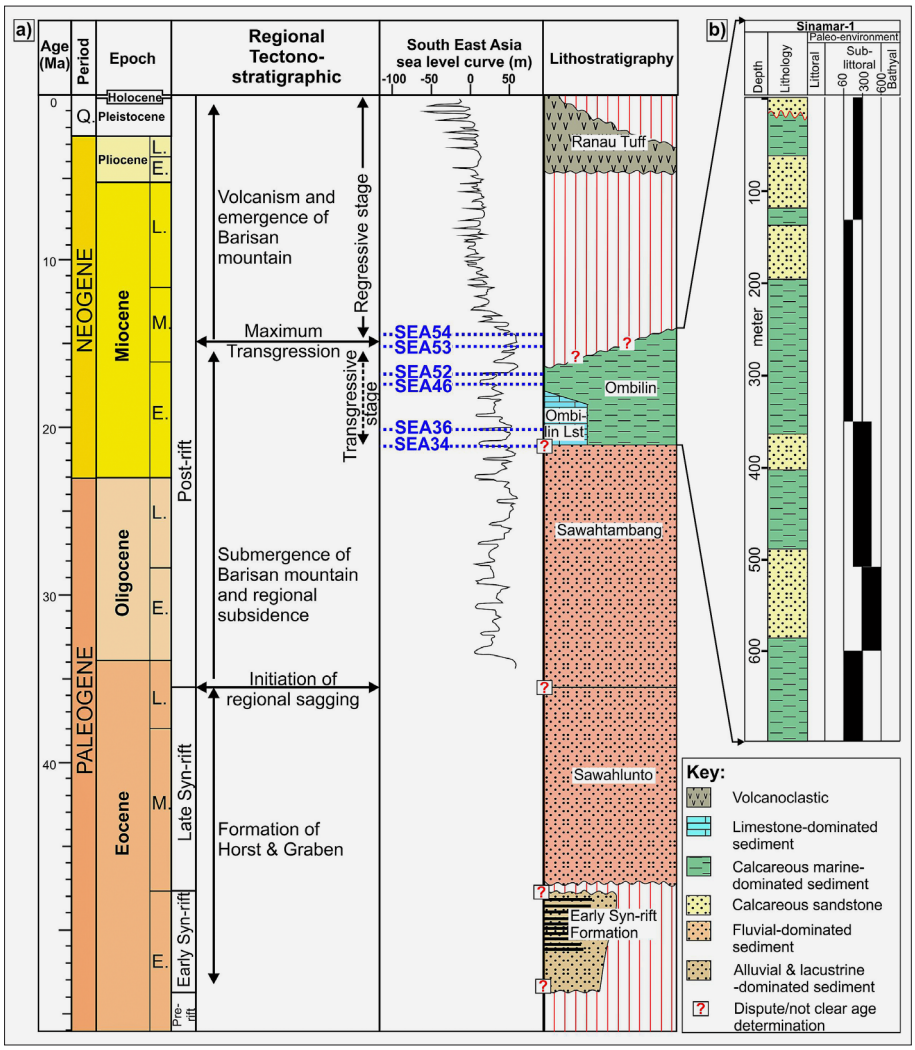

Figure 2. a) Simplified regional tectono- and lithostratigraphy in the Ombilin Basin according to **Noeradi et al (2005)** and **Barber et al (2005)**, modified to accommodate the latest published age of early syn-rift (Early Eocene) and Sawahlunto Formation (Middle-Late Eocene) from **Murray (2020)**. b) Mudlog of Sinamar 1, covering the Ombilin Formation and its paleoenvironment based on biostratigraphy data (**Koning, 1985**). See the location of Sinamar-1 in **Figure 1**.

During the late post-rift phase, the Ombilin Formation and Ranau Tuff were deposited (**Koesoemadinata and Matasak, 1981; Noeradi et al., 2005**), with the Ombilin Formation unconformably (**Koning, 1985; Whateley and Jordan, 1989**) or conformably (**Fletcher and Yarmanto, 1993; Noeradi et al., 2005**) overlying the Sawahtambang Formation (**Figures 1b-d** and **2**). Although initially reported only in the Sinamar sub-basin, which extends laterally from Batumanjulur near the Tanjung Ampalu Fault to the eastern margin of the sub-basin (**Koning, 1985; Anastasia et al., 2012**), the Ombilin Formation has also been identified in the Talawi sub-basin (**Linggadipura et al., 2018**). Seismic data indicate this formation has a thickness of approximately 2740–4000 m in the northern limb of the basin (**Koning, 1985; Anastasia et al., 2012**), while up to 692 m was encountered in the Sinamar-1 **(Fletcher and Yarmanto, 1993; Noeradi et al., 2005; Figure 2**). However, the true thickness of this formation remains uncertain due to post-depositional erosion. The lower part of the formation is marked by calcareous mudrock with limestone nodules and thin foraminiferal limestone lenses or beds (**Koesoemadinata and Matasak, 1981; Howells, 1997; Anastasia et al., 2012**), which grades upward into carbonaceous, calcareous, and silty to sandy mudrocks interbedded with sandstone and/or tuff (**Koesoemadinata and Matasak, 1981; Noeradi et al., 2005; Habrianta et al., 2018**). The sandstones are typically very fine- to fine-grained, calcareous, and glauconitic (**Noeradi et al., 2005**). The deposition of this formation has been interpreted as neritic to bathyal in the Sinamar Sub-basin, based on biostratigraphic data (e.g. **Koesoemadinata and Matasak, 1981; Koning, 1985**). In contrast, a transitional environment has been suggested for the Talawi Sub-basin (**Linggadipura et al., 2018**). Deposition of this formation coincided with the continued uplift of the Barisan Mountains (**Moss and Carter, 1996; Barber et al., 2005; Erdi et al., 2025**), volcanic activity in the basin's northeastern margin (**Koesoemadinata and Matasak, 1981**), and regional subsidence (**Howells, 1997**).

Following the deposition of the Ombilin Formation, the Ranau Tuff was locally deposited and is unconformably overlying the Ombilin Formation within the Ombilin Basin (**Figures 1b and 2; Koesoemadinata and Matasak, 1981; Habrianta et al., 2018**). This tuff unit has been interpreted to have been deposited during the Pleistocene (**Koesoemadinata and Matasak, 1981; Habrianta et al., 2018**), or from the Pliocene to Recent

(**Fletcher and Yarmanto, 1993**). It is composed of andesitic to basaltic lava flows, lahar deposits, and tuffs (**Fletcher and Yarmanto, 1993**).

3. Methods

Two methods were conducted in this study, consisting of sedimentary logging and petrographic analysis. The sedimentary logging was conducted to uncover sedimentary characteristics, while petrographic analysis was conducted to unravel sandstone characteristics and the provenance of the Ombilin Formations.

3.1. Sedimentary Logging

Geological data were collected through three measured outcrop sections located within a 12 km radius of Sijunjung, West Sumatra, specifically in the Sinamar Sub-basin (see **Figure 1b**). The outcrops, aligned with the regional N–S strike of the Tanjung Ampalu Fault, provided excellent vertical but limited lateral exposures. Two localities, which are Wali Nagari Bukit Bual and Sungai Batang Ombilin, were examined, and approximately 80 m of the Ombilin Formation was measured. In this study, higher-resolution logging was conducted to document sedimentary features for facies analysis, including grain size, sorting, roundness, color, sedimentary structures, bed thickness, fossil content, and bounding contacts. Facies and facies associations were interpreted based on lithology, sedimentary structures, and vertical stacking patterns following standard methodologies (**e.g. Anderton, 1985; Zakaria et al., 2013**).

3.2. Petrography, Sandstone Classifications and Provenance

Twenty petrographic samples were collected from the measured outcrop sections of the Ombilin Formation, of which seven were selected for detailed petrographic analysis. The seven samples were used to illustrate (1) non-calcareous, sand-rich sediments, (2) sandy calcareous sediments, and (3) limestone, which collectively reflect the sedimentary compositions of the Ombilin Formation. Thin sections were prepared from these samples, impregnated with blue-stained epoxy resin to enhance porosity visualization, and examined under a transmitted light petrographic microscope (Zeiss Axio Imager A2m). Detrital components (e.g. quartz, feldspars, lithic fragments), authigenic minerals (e.g. heavy and accessory minerals, silicates), biogenic materials (e.g. bioclasts), matrix, and cement were identified. Petrography was employed as a primary method for provenance analysis, in line with standard practices for initial sandstone provenance studies (**e.g. Augustsson, 2021**). Sandstone composition was recalculated using point counting to generate ternary plots for classification and provenance purposes (**e.g. Dickinson, 1985; Malaza et al., 2015**). These data were plotted on QFL diagrams of **Pettijohn (1975)**, **Folk (1980)**, and **Dickinson et al. (1983; 1985**) to infer sandstone classifications, tectonic settings, and sedimentary provenances.

4. Results

The methodology outlined previously was applied, and the results are presented in this chapter. The findings comprise descriptions of facies associations and petrographic characteristics of the Ombilin Formation.

4.1. Facies Associations of the Ombilin Formation

Ten lithofacies were identified based on distinctive features such as grain size, sorting, roundness, sedimentary structures, fossil content, and bedform-to-outcrop geometry (C1–C3 and S1–S7; **Figure 3 and Table 1**). These were grouped into three facies associations (FA1–FA3) according to their characteristics, occurrence, and vertical stacking patterns (see **Figure 3** and **Table 2**). FA1 were observed in sections C and D, situated southward and northeastward of section B. The FA2 and FA3, however, were recognized in sections B, located east of the Tanjung Ampalu Fault (see **Figure 1b**). Strike-projection onto a cross-section indicates that section B lies between sections C and D and is separated by subsurface normal faults, although no surface expression of these faults, such as repetition of sedimentary log, was observed during logging (see **Figure 1c**). This stratigraphic relationship suggests that FA1 in section C is older than the FA2 and the FA3, while FA1 in section D is younger than the FA2 and the FA3 in section B (see **Figure 3**). The three facies associations are described in detail below.

4.1.1. Facies Association 1 (FA1)

The FA1 is comprised of three lithofacies, being represented by alternations of calcareous mudrock (C1), calcareous ripple-stratified sandstone (C2), and stratified limestone (C3; **Figure 3** and **Table 2**). The C1 is defined by up to 8 m thick, dark grey, silt-grained, calcareous mudrocks, containing shell fragments and locally displaying parallel laminations (C1; **Figure 4a–c** and **Tables 1–2**). Sharp contacts are observed at both the base and top of the C1 with either the C2 or the C3 within FA1, while locally, the top surface is truncated by an erosional contact with the S1 of the FA2 (see **Figure 3**).

Facies C2 is observed in alternation with the calcareous mudrock of C1 within FA1 (see **Figure 3** and **Tables 1–2**). The C2 is defined by up to approximately 0.5 m thick, greenish light grey, well-sorted, rounded, very fine- to fine-grained calcareous sandstones containing glauconite and displaying internal parallel and ripple laminations (see **Figure 4d**). Sharp contacts are present at both the base and top of the C2, with the adjacent C1 within FA1.

The final facies within the FA1 is the C3, occurring as alternations with C1 (see **Figure 3** and **Tables 1-2**). It is

Table 1. Sedimentary facies of the Ombilin Formation

Facies name and code	Textures	Thickness (m)	Sedimentary structure	Trace fossils and biota	Interpretation
Calcareous, massive mudrock (C1)	Dark grey, lime mudrock, showing silt-grained mudrock (Fig. 9a-c).	0.3-8 m thick.	Structureless	Shell fragments	Combination of breakdown of calcareous bioclast (**Pratt, 2010**), suspension, and/or dynamic process of long-distance horizontal transport of mud aggregates (**Plint, 2010**).
Calcareous, ripple-stratified sandstone (C2)	Greenish light grey, rounded and well sorted, very fine to medium-grained sandstone, containing glauconite and bioclasts.	0.1 - 0.5 m thick	Parallel-, and commonly symmetric ripple laminations		Combination of breakdown of calcareous bioclasts and episodic oscillatory current (**e.g. Pratt, 2010**). The glauconite reflects the boundary condition of oxidizing seawater and reducing interstitial water at depths of down to 60 m (**e.g. Odin and Matter, 1981**).
Stratified limestone (C3)	Horizontally stratified, grain-supported, fine to medium-sized sandy skeletal limestone, being classified as packstone	up to 1.5 m thick	Parallel stratification		Depositional product of a deep ramp of a shallow carbonate platform, being controlled by subtidal cycles (**Jones, 2010**).
Amalgamated sandstone (S1)	Reddish brown, sub-rounded to rounded, poorly sorted, gravel-grained conglomerates. The conglomerates contain igneous rocks and mud clasts that contain plant and/or coal fragments	Up to 0.8 m thick; occurring close to the base of the sedimentary bed.	Vertically amalgamated and fining upward. Internally show coal stringer and parallel lamination at the top.	Plant fragments	Basal gravel-grained conglomerate reflects lag deposits, being related to migration of channel thalweg and dunes (**e.g. Plink-Bjorklund, 2005; Fakhruddin et al., 2023**). The amalgamated geometry indicates a high rate of sedimentary discharge (**e.g. Boggs, 2014**). The parallel lamination reflects the transition of upper flow into lower flow regime (**Boggs, 2014**). The laminated mudrock deposited due to suspension, while coal stringer reflects rapid accumulations of plant fragments and peats (**Plink-Bjorklund, 2005**).
	Reddish brown, sub-rounded to rounded, poorly sorted, fine to coarse-grained sandstones.	Up to 0.7 m thick.			
	White grey, claystone.	Laminated up to 1 cm thick; occurring at the top of the sandstones.			
Interbedded sandstone and mudrock (S2)	Reddish brown, sub-angular to sub-rounded, poorly sorted, fine to coarse-grained sandstones.	Up to 0.6 m thick.	Parallel lamination	-	Planar bed flows of the upper flow regime in point bars (**e.g. Plink-Bjorklund, 2005; Boggs, 2014**).
	Light yellowish grey, silt-grained mudrock, locally shows coal stringers.	Up to 0.3 m thick.			
Massive sandstone (S3)	Reddish brown, medium to thick bed, sub-rounded to rounded, poorly sorted, broadly fine to coarse-grained sandstones.	Up to 7 m thick.	Structureless	Occasionally plant fragments; Locally shell fragment.	High and rapid depositional rates and various intensity of high concentration and energy in depositional environments (**e.g. Olariu et al., 2010; Fakhruddin et al., 2023**).
Cross-stratified sandstone (S4)	Reddish brown to yellowish grey, sub-rounded to rounded, poorly sorted, fine to coarse-grained sandstones.	0.3-0.6 m thick.	Planar and herringbone cross stratifications	-	Planar cross-stratifications reflect downstream migration of 2D dunes and/or migration of longitudinal bars in channels; Herringbone cross-stratifications reflect migration of 3D dunes in channels, bidirectional currents of approximately equal strength (**e.g. Plink-Bjorklund, 2005; Fakhruddin et al., 2023**).

Table 1. Continued

Facies name and code	Textures	Thickness (m)	Sedimentary structure	Trace fossils and biota	Interpretation
Heterolithic bedding (S5)	Yellowish grey, rounded and well sorted of laminated and/or thin beds of reddish brown, fine to coarse-grained sandstone; Locally show coal stringers.	Laminated sandstones alternating with mudrock; Both occurs of up to 0.1 m thick.	Wavy lamination and/or flaser	Plant fragments	Depositions from reversing tidal currents (**Reineck and Singh, 1980**), suggesting an intertidal succession of decreasing current energy (**e.g. Dalrymple, 1992**).
	Light yellowish grey, claystone.				
Ripple-stratified sandstone (S6)	Yellowish grey, sub-rounded to rounded, poorly sorted, fine to coarse-grained sandstones	Up to 0.4 m thick.	Locally parallel and commonly symmetric ripple laminations	*Skolithos* and *Laevicyclus*	Symmetric rippled stratifications represent lower flow regime (**e.g. Simons and Richardson, 1963; Boggs, 2014; Fakhruddin et al., 2023**), being deposited during maximum tidal flow (**e.g. Plink-Bjorklund, 2005**); The locally parallel lamination reflects deposition from traction current (**e.g. Boggs, 2014; Plink-Bjorklund, 2005**). The *Skolithos* and *Laevicyclus* indicates deposition in shallow marine and/or nearshore environments, being influenced by tidal currents (**e.g. Desjardins et al., 2012; Knaust et al, 2018**).
Massive mudrock (S7)	Light yellowish grey, silt-grained mudrock. Locally show coal stringers.	Up to 2.7 m thick.	Structureless	-	Depositions from suspensions in low-energy environments (**e.g. Santos and Rossetti, 2006; Fakhruddin et al., 2023**).

characterized by up to 1.5 m thick, yellowish light grey, grain-supported, presence of carbonate mud, horizontally stratified limestone (see **Figure 4c**). Their character of grain-supported with carbonate mud is shown, suggesting packstone of **Dunham's (1962)** classification. Sharp contacts are observed at both the top and base of the C3 with the adjacent C1 facies within FA1 (see **Figures 3** and **4c**).

4.1.2. Facies Association 2 (FA2)

The FA2 is composed of four lithofacies, typically represented by alternations of amalgamated sandstone (S1), interbedded sandstone and mudrock (S2), massive sandstone (S3), and/or cross-stratified sandstone (S4) (see **Figure 3** and **Table 2**). The lithofacies S1 occurs interbedded with the S3 and/or the S4 and is characterized by conglomerate beds at the base, overlain by fining-upward, amalgamated sandstones (S1; **Figure 5a–c** and **Table 1-2**). The conglomerates, up to approximately 0.8 m thick, are reddish-brown, poorly sorted, and composed of sub-rounded to rounded gravel clasts, including igneous rock and mudrock fragments with plant remains and coal (see **Figure 6a**). The overlying sandstones are up to 0.7 m thick, reddish-brown, and similarly poorly sorted, containing fine- to coarse-grained, sub-rounded to rounded grains. Parallel lamination and local laminated mudrock and coal stringers occur at the top of the sandstone beds (see **Figure 6b**), with white-grey claystone being up to 1 cm thick. The basal contact of the S1 is typically erosional against the S2 and the S3 of the FA2, or calcareous mudrock (C1) of the FA1, but is sharp against the S4 within the FA2 (see **Figure 3**). Its overlaying contact is sharp with either S3 of the FA2 or the heterolithic bedding (S5) of Facies Association 3 (FA3).

Lithofacies S2 is defined by interbedded sandstone and mudrock and occurs alternating with S3 and/or S4 (S2; **Figures 3, 5b, d,** and **Tables 1-2**). The sandstones reach up to 0.6 m thick, are reddish-brown, poorly sorted, and composed of fine- to coarse-grained, sub-angular to sub-rounded particles, exhibiting parallel lamination (see **Figure 5b, d**). The mudrocks, up to 0.3 m thick, are light yellowish, massive, and composed of silt-grained materials. The basal contact of the S2 is sharply defined against the underlying S1, the S3 of the FA2, or the S5 of the FA3. The upper boundary of the S2, however, is sharp against the overlying S3 of the FA2 or ripple-laminated sandstones (S6) and massive mudrocks (S7) of the FA3 (see **Figure 3**).

Lithofacies S3 is defined by massive and structureless sandstones and occurs either as a singular facies or in alternation with S1, S2, and/or S4 (S3; **Figures 3, 5a, e,** and **Tables 1-2**). This lithofacies S3 is characterized by reddish-brown, massive, poorly sorted sandstones, up to 7 m thick, composed of fine- to coarse-grained, sub-rounded to rounded particles. The basal contacts of the S3 are sharply defined against the S1, the S2, or the S4 of the FA2, and the S7 of the FA3 (see **Figure 3**). The

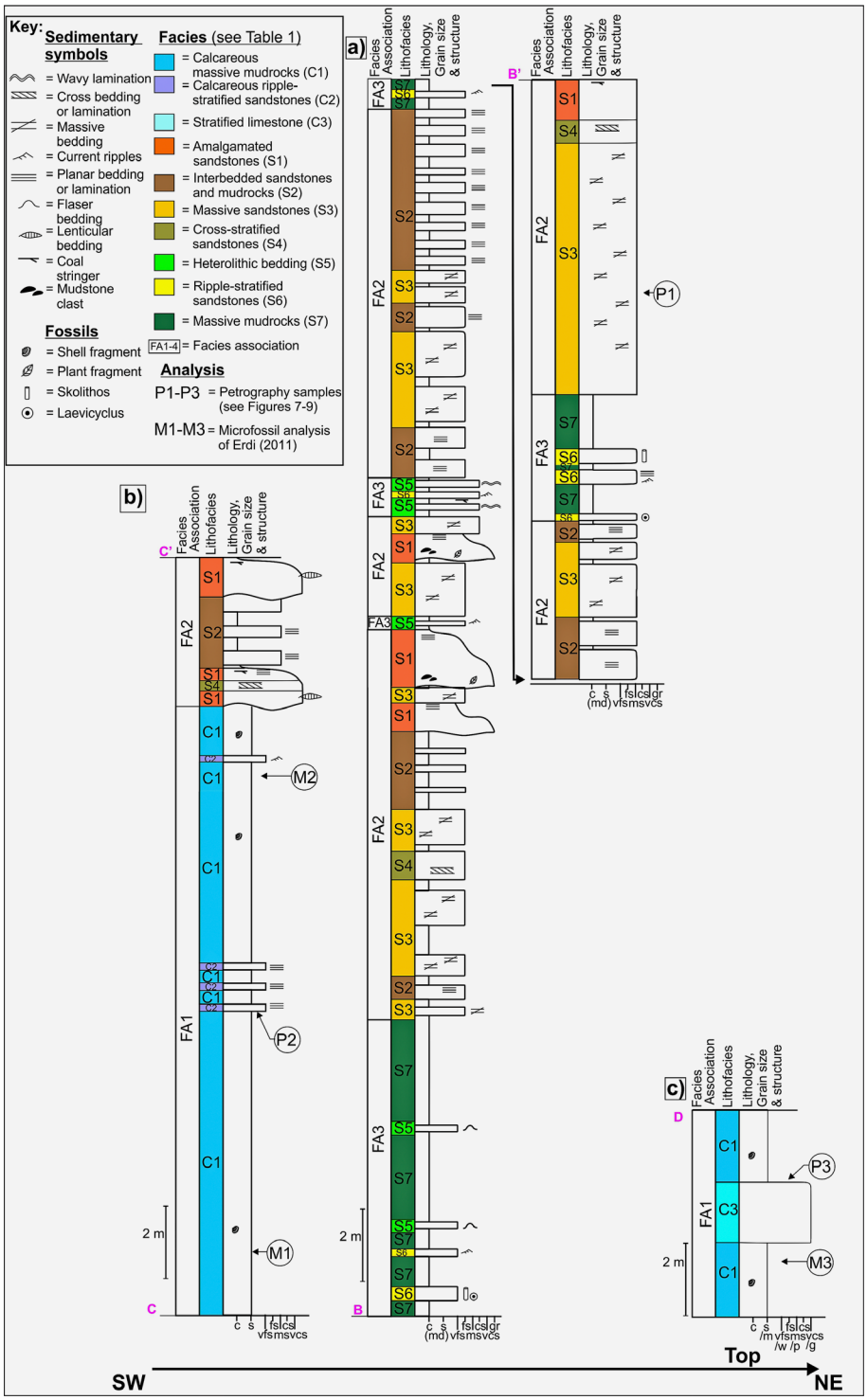

Figure 3. Sedimentary log of the Ombilin Formation in this study, being measured in Wali Nagari Bukit Bual, Sijunjung Province in section B-B' and D-D' (a, c) and Sungai Batang Ombilin in section C-C (b). Strike-projection of the measured log in **Figure 1b** onto A-A' section (see **Figure 1c**) shows that the measured log of C-C', B-B' and D reflect the Ombilin Formation from bottom to top. The petrographic samples are recorded on S_3, C_2, and C_3 for P_1, P_2, and P_3, respectively. The biostratigraphic samples of **Erdi (2011)** are recorded on C_1 for M_1 and M_2.

Table 2. Facies associations (FA) of the Ombilin Formation

Facies Association and code	Lithofacies	Interpretation
Facies Association 1 (FA1)	C1, C2, C2	Open marine
Facies Association 2 (FA2)	S1, S2, S3, S4	Tidal channel
Facies Association 3 (FA3)	S5, S6, S7	Mixed tidal flat

upper contacts of the S3 are also sharp, occurring against the S2 or the S4 of the FA2, or the S5 and the S7 of the FA3. Still, the S3 locally has erosion contact with the overlying S1 sandstones of the FA2.

The final facies within the FA1 is represented by lithofacies S4, being defined as cross-stratified sandstones and observed in alternation with S1, S2, and/or S3 (see **Figure 3** and **Tables 1-2**). This lithofacies S4 is characterized by reddish-brown, poorly sorted, fine- to coarse-grained sandstones up to 0.6 m thick, composed

Figure 4. Field photographs illustrating the characteristics of facies association 1 (FA1), showing: (a) thick sequence of calcareous mudrock (C1); (b) presence of shell fragments in the C1; (c) interbedding of the C1 and stratified limestone (C3); (d) presence of calcareous ripple-stratified sandstone (C2).

of sub-rounded to rounded grains (see **Figures 3** and **4e; Table 1**). Planar and herringbone cross-stratifications are present within the sandstones of the S4 (see **Figures 5e** and **6d**). The basal contact is sharp against the S3, while the upper boundary is sharply defined against either the S1 or the S3 within the FA2 (see **Figure 3**).

4.1.3. Facies Association 3 (FA3)

The FA3 is defined by three lithofacies, typically represented by a singular S5, or occasionally by alternations between heterolithic bedding (S5), ripple-laminated sandstones (S6), and/or massive mudrocks (S7; **Figure 3** and **Tables 1-2**). The S5 facies is marked by up to 2 m thick heterolithic bedding, composed of interlaminated sandstones and claystone. The sandstones are characterized by reddish-brown, well-sorted, rounded, fine- to coarse-grained laminations, each up to 1 cm thick, and internally display wavy and flaser bedding (see **Figure 6e; Table 1**). In contrast, the claystone is distinguished by light yellowish-grey, massive, clay-textured laminations of similar thickness. The base of the S5 is bounded sharply by either the S7 of the FA3 or the massive sandstones (S3) of FA2, while the top is typically in a sharp contact with either the S7 of FA3 or the S2 of FA2 (see **Figure 3**). Locally, the top contact is erosional, overlying the S1 of the FA2.

The S6 is made of symmetric ripple-laminated sandstones, typically occurring in alternation with S5 and/or S7 within FA3 (see **Figure 3; Tables 1–2**). This facies is characterized by up to 0.4 m thick, yellowish-grey, poorly sorted, sub-rounded to rounded, fine- to coarse-grained sandstones, internally showing symmetric ripple and parallel laminations, and locally containing abundant bioturbations (see **Figure 6f–h**). The bioturbations show cylindrical burrows of up to 0.5 cm in diameter, filled with fine-grained sand and enclosed by medium- to coarse-grained sands, interpreted as *Skolithos linearis* (**cf. Knaust, 2015; Knaust et al., 2018; Figure 6g**). Other bioturbations consist of cylindrical burrows with fine-grained sandy cores and surrounded by fine- to medium-grained friable sandstone, resembling *Laevicyclus*

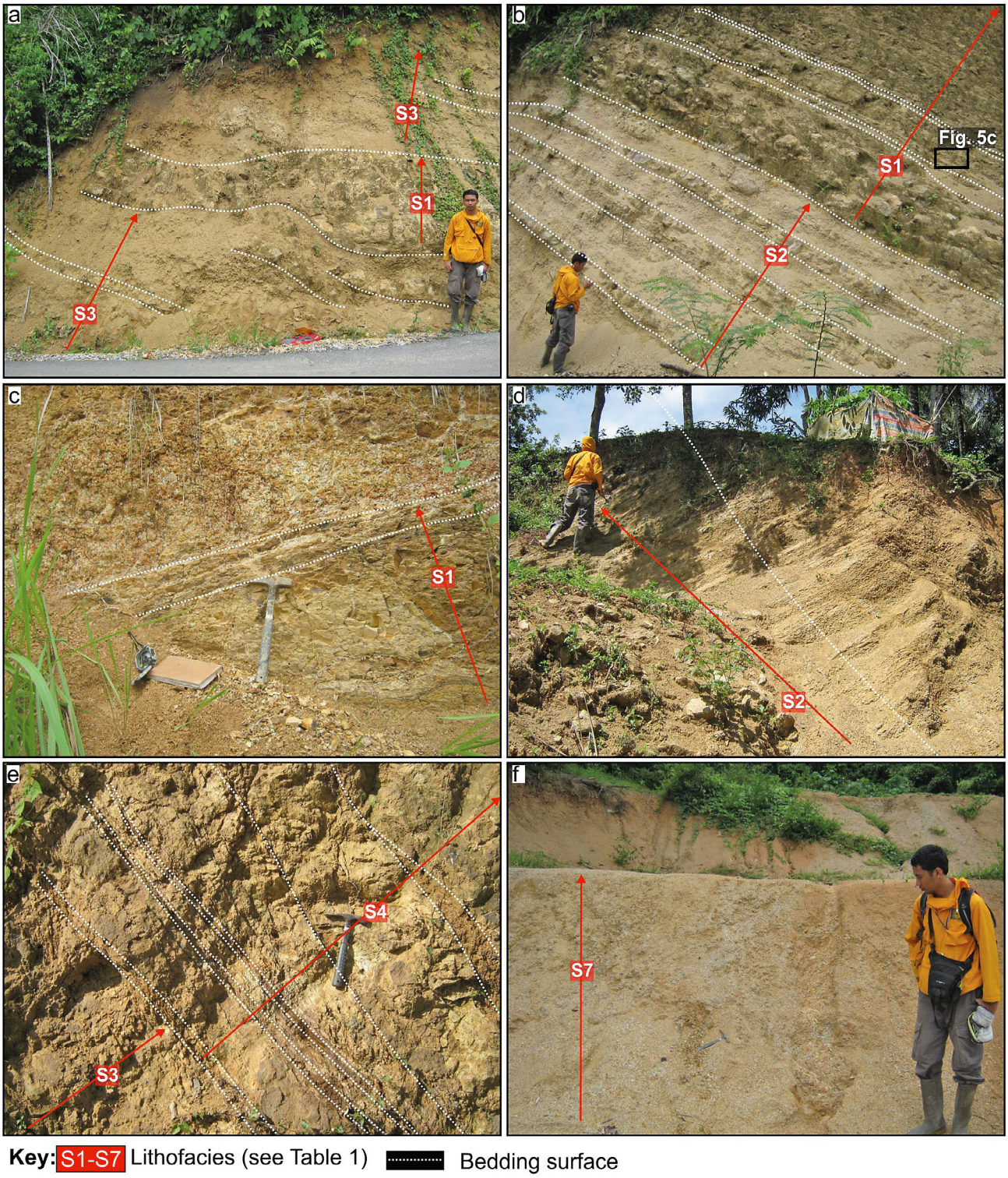

Figure 5. Field photographs illustrating the characteristics of: (a-e) facies association 2 (FA2) that consists of amalgamated sandstone (S_1), interbedded sandstones and mudrocks (S_2), massive sandstones (S_3), cross-stratified sandstones (S_4), and (f) facies association 3 (FA3) that consists of massive mudrocks (S_7).

parvus (**cf. Knaust, 2015; Knaust et al., 2018; Figure 6h**). The base of the S6 is marked by a sharp contact with the S7 of FA3, while the top contact is sharp against either the S3 of FA2 or the S7 within FA3 (see **Figure 3**).

The final facies identified within FA3 is the S7, which is composed of massive mudrock (S7; **Figures 3, 5f,** and **Tables 1-2**). This facies alternates with S5 and S6. The S7 is characterized by up to 3 m thick, light yellowish-grey, massive, silt-grained mudrock. The base of the S7 is marked by a sharp contact with either the S2 or S3 of FA2, or with S5 or S6 within FA3. The top of the S7 is also similarly bounded by sharp contacts

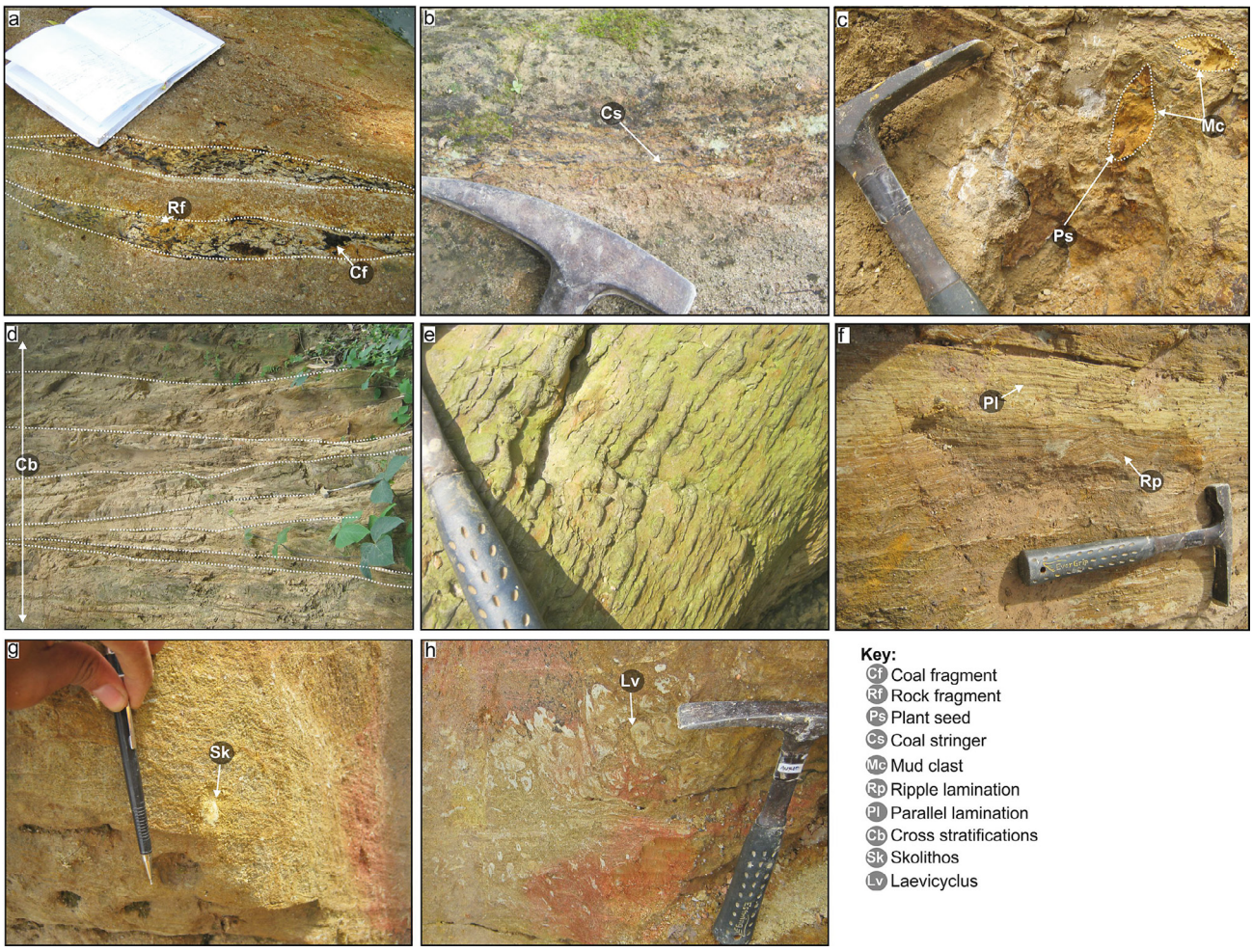

Figure 6. Characteristics of facies association 2 (FA2) and facies association 2 (FA3). The FA2 is characterized by: (a) mud clasts, including coal fragments, in S1; (b) parallel lamination with coal stringer in S1; (c) plant fragment in S1; and (d) herringbone structures in S4. The FA2, however, is characterized by: (e) flaser bedding in S5; (f) parallel and symmetric ripple laminations in S6; and trace fossils in S6 such as (g) *Skolithos* and (h) *Laevicyclus*.

with the S3 of FA2 or with S5 or S6 within FA3 (see **Figure 3**).

4.2. Petrography of the Ombilin Formation

Petrography analyses were conducted to unravel the texture and composition of sandstone and limestone in the Ombilin Formation. Three selected petrography analysis was presented, given these three samples reflect non-calcareous, sand-rich sediment, sandy calcareous sediments, and limestone. Petrography of non-calcareous, sand-rich sediment was reflected by the S3. On the other hand, the petrography of sandy calcareous sediments was illustrated by C2, while the limestone was reflected by the C3.

4.2.1. Petrography of C2

Petrographic analysis of the C2 facies within the FA1 was performed to determine the texture and composition of calcareous, ripple-stratified sandstones in the Ombilin Formation (P2; **Figure 3**). The C2 is consists of averages of 0.8% quartz, 30.8% feldspar, 5.3% lithic fragments, 30.1% bioclasts, 23.7% accessory minerals, 2.4% silicate minerals, 4.8% matrix, and 2.1% cement (see **Figure 7; Table 3-4**). Grain sizes range from 0.1 to 0.45 mm, indicating a very fine- to medium-grained sandstone according to **Wentworth's (1922)** classification.

Detrital minerals in the C2, including quartz, feldspar, and lithic fragments, exhibit compositional variability (see **Figure 7; Table 3**). The quartz is generally rare, with some samples completely lacking it. When present, the quartz contains monocrystalline grains. Feldspar, however, dominates the detrital framework. These grains are sub-rounded and usually display linear or point contacts. Lithic fragments are mostly of volcanic origin, characterized by sub-angular to sub-rounded shapes and long contacts with adjacent grains (see **Figure 7e–f**). Normalized point counting was conducted to determine percentages of QFL compositions in the C2, showing feldspar, quartz, and lithic fragments average making up 77.3%, 1.4% and 21.27% of the framework, respectively (see **Table 5**).

Table 3. Summary of composition and texture of petrography from the Ombilin Formation.

Sample	Composition		Textures and features
Calcareous, ripple-stratified sandstone (C2)	Quartz		Grain size: from 0.1 to 0.2 mm (very fine- to fine-grained)
			Shape: mostly sub-rounded
			Strained: high strained
			Contact: linear and point contact
	Feldspar		Grain size: from 0.1 to 0.45 mm (very fine- to medium-grained)
			Shape: mostly sub-rounded
			Contact: linear and point contact
	Lithic fragments	Volcanic fragment	Grain size: from 0.3 to 0.4 mm (medium-grained)
			Shape: sub-angular to sub-rounded
			Contact: long contact
	Bioclast		Grain size: from 0.18 to 0.3 mm (fine- to medium-grained)
			Occurrences: foraminiferal skeletal fragments
	Accessory mineral	Glauconite	Grain size: average of 0.2 mm (fine-grained)
			Occurrences: act as grains; commonly interlock with feldspars
		Chlorite	Grain size: average of 0.2 mm (fine-grained)
			Occurrences: as detrital monomineralic grains
	Silicate mineral	Pyroxenes	Grain size: average of 0.2 mm (fine-grained)
			Occurrences: act as grains; commonly form prismatic shape
	Matrix	Calcite	Occurrences: filling intergranular pore spaces; locally replaces bioclast shells
	Cement		
Stratified limestone (C3)	Quartz		Grain size: from 0.08 to 0.2 mm (very fine- to fine-grained)
			Shape: rounded
			Strained: moderate-high strained
			Contact: linear and point contact
	Feldspar		Grain size: from 0.08 to 0.2 mm (very fine- to fine-grained)
			Shape: rounded
			Contacts: linear and point contacts
	Bioclast		Grain size: from 0.18 to 0.3 mm (fine- to medium-grained)
			Occurrences: foraminiferal skeletal fragments
	Calcite		Occurrences: replacement of bioclast material
	Micrite		Occurrences: filling intergranular pore spaces
	Sparry calcite		
Massive sandstone (S3)	Quartz		Grain size: from 0.3 to 0.5 mm (fine- to coarse-grained)
			Shape: mostly sub-rounded
			Strained: moderate-high strained
			Contacts: linear and concave-convex contacts
	Feldspar		Grain size: from 0.2 to 0.6 mm (fine- to coarse-grained)
			Shape: sub-angular to sub-rounded; prismatic shapes
			Contacts: linear contacts
	Lithic fragments	Volcanic fragment	Grain size: from 0.4 to 0.6 mm (medium- to coarse-grained)
			Shape: sub-angular to sub-rounded
			Contacts: linear contacts
	Accessory Mineral	Muscovite	Grain size: from 0.2 to 0.3 mm (fine- to medium-grained)
			Shape: sub-rounded to rounded
			Alterations: expanding into pore spaces and grow from grains
		Opaque	Occurrences: commonly as coating and stains on quartz grains
	Matrix	Very fine lithic fragment and clay minerals	Occurrences: fill pore spaces and occur as coating on grains
	Cement	Very fine calcite	Occurrences: cement-filling grain contacts
		Very fine muscovite	
		Oxide mineral	

Table 4. Summary of point counting results of compositions in petrography samples from the Ombilin Formation. The compositions for sandstones are defined for **Zuffa (1980)** scheme. The Zuffa code reflect non-carbonate extrabasinal (NCE), carbonate intrabasinal (CI), non-carbonate intrabasinal (NCI), carbonate matrix (CMt), carbonate cement (CCm) and non-carbonate cement (NCCm).

Sample	Composition		Proportion (%)			Average (%)	Classifications of Zuffa (1980)		
			Sub-Sample						
			1	2	3		Spatial	Compositional	Zuffa (1980) code
Calcareous, ripple-stratified sandstone (C2)	Quartz		0	2	0.4	0.8	Extrabasinal	Non-carbonate	NCE
	Feldspar		31	30.6	30.8	30.8	Extrabasinal	Non-carbonate	NCE
	Lithic fragments	Volcanic fragment	5.5	5	5.4	5.3	Extrabasinal	Non-carbonate	NCE
	Bioclast		30.8	29.5	30	30.1	Intrabasinal	Carbonate	Cl
	Accessory mineral	Glauconite	20	21.4	20.5	20.63	Intrabasinal	Non-carbonate	NCl
		Chlorite	3	2.2	4	3.07	Extrabasinal	Non-carbonate	NCE
	Silicate mineral	Pyroxenes	2.7	2.5	2	2.4	Extrabasinal	Non-carbonate	NCE
	Matrix	Calcite	5	4.6	4.8	4.8	Intrabasinal	Carbonate	CMt
	Cement		2	2.2	2.1	2.1			CCm
Stratified limestone (C3)	Quartz		7			7			
	Feldspar		3			3			
	Bioclast		20			30			
	Calcite		20			10			
	Micrite		35			35			
	Sparry calcite		15			15			
Massive sandstone (S3)	Quartz		8.6	10.7	10.4	9.9	Extrabasinal	Non-carbonate	NCE
	Feldspar		58.6	57.8	55.1	57.17	Extrabasinal	Non-carbonate	NCE
	Lithic fragments	Volcanic fragment	15.6	14.8	12.3	14.23	Extrabasinal	Non-carbonate	NCE
	Accessory Mineral	Muscovite	3.2	2.3	3.9	3.13	Extrabasinal	Non-carbonate	NCE
		Opaque	5	7	6	6	Intrabasinal	Non-carbonate	NCl
	Matrix	Very fine lithic fragment and clay minerals	2	2.4	5	3.13	Extrabasinal	Non-carbonate	NCE
	Cement	Very fine calcite and muscovite	2	2.8	3	2.6	Intrabasinal	Carbonate and non-carbonate	CCm and NCCm
		Oxide	5	2.2	4.3	3.83	Intrabasinal	Non-carbonate	NCCm

Table 5. Average of normalized point counting results (percentage) for Petrographic sample from the Ombilin Formation.

Facies	Sample Number	Q	F	L	Avg. Q	Avg. F	Avg. L	Qm	Qp	Avg. Qm	Avg. Qp
C2	1	0	76.8	23.2	1.4	77.3	21.27	0	0	1.4	0
	2	3.1	78	18.9				3.1	0		
	3	1.1	77.2	21.7				1.1	0		
S3	4	9.8	73.3	16.9	11.67	70.87	17.5	8.2	1.6	9	2.6
	5	12.7	71.5	15.8				9.6	3.1		
	6	12.4	67.8	19.8				9.2	3.2		

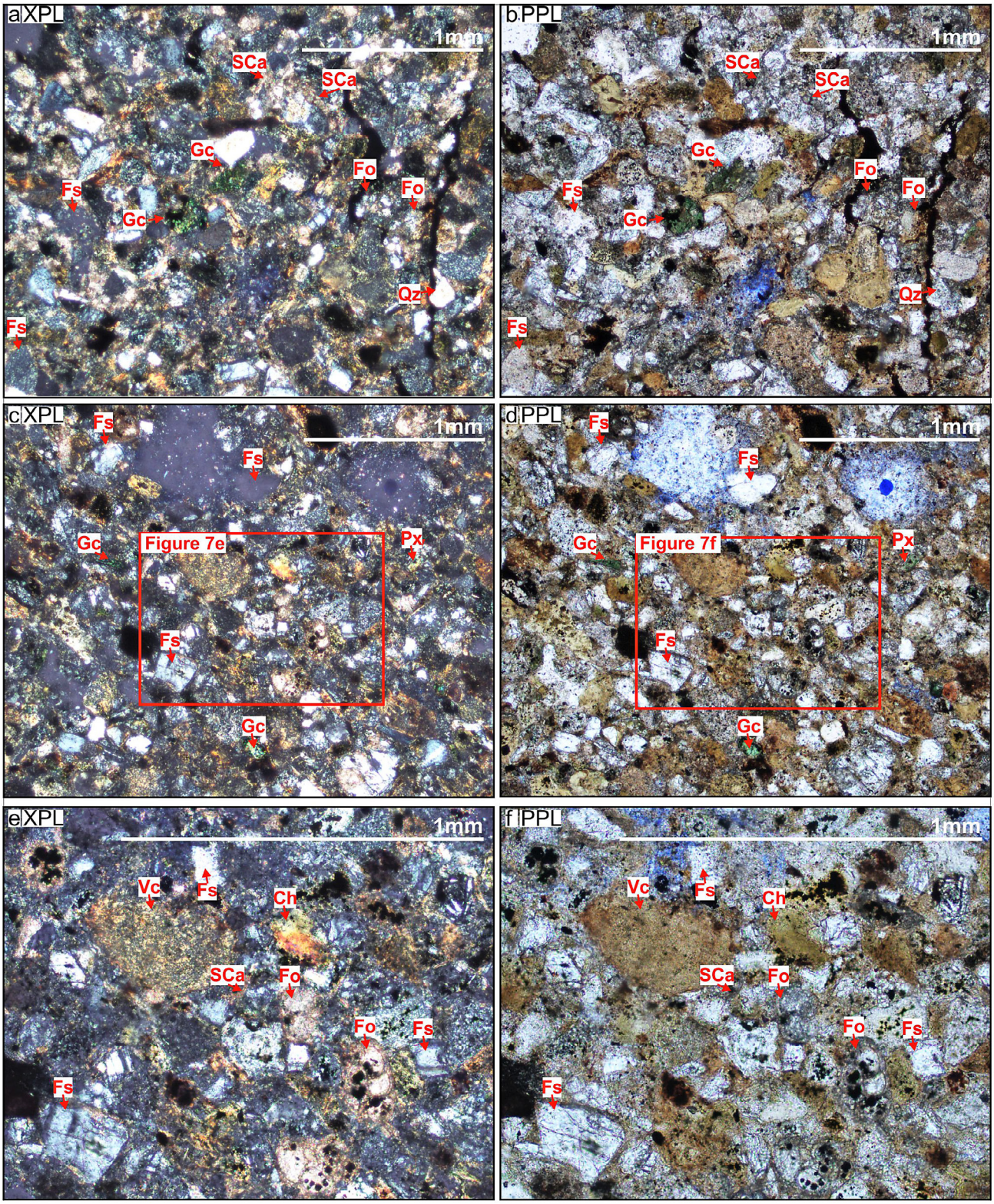

Figure 7. Photomicrographs from thin sections of calcareous ripple-stratified sandstones (C2) of facies association 1 (FA1) in the Ombilin Formation, being taken from P2 (see **Figure 3**). The thin sections show (a) cross- and (b) parallel- polarized with 10x magnifications, showing the characteristic of the C2. The C2 in (a) and (b) composed of quartz (Qz), feldspar (Fs), bioclast (Fo), glauconite (Gc) and sparry calcite (SCa). The thin sections also show (c) cross- and (d) parallel-polarized with 10x magnifications, and (e) cross- and (f) parallel-polarized with 25x magnifications. The (c-f) show volcanic fragments (Vr), chlorite (Ch), and pyroxene (Px) along sparry calcite (SCa).

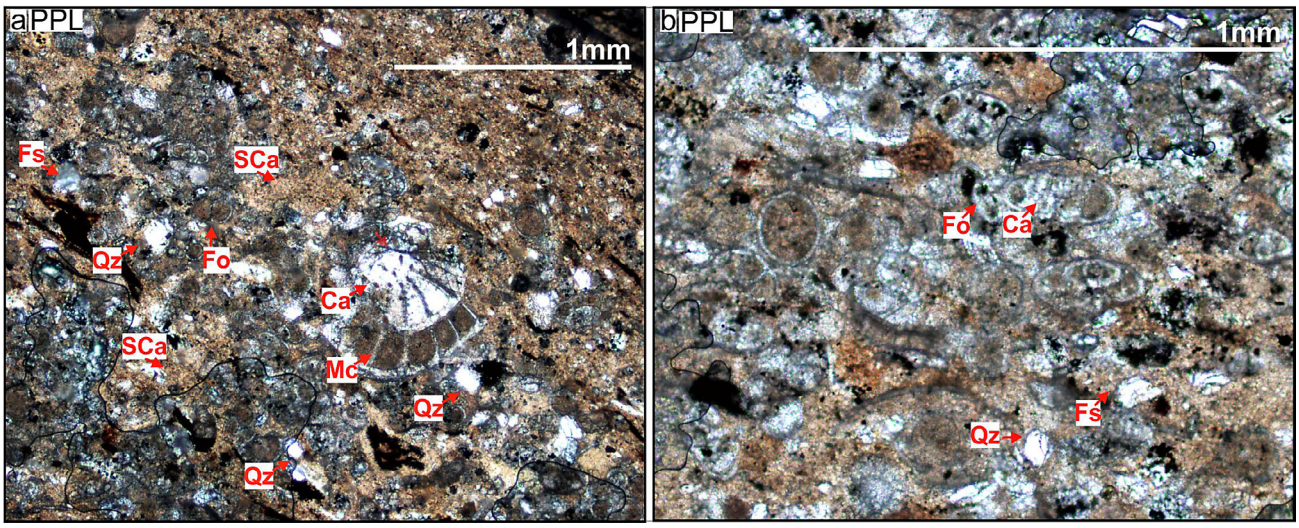

Figure 8. Photomicrographs from thin sections of stratified limestone (C3) of facies association 1 (FA1) in the Ombilin Formation, being taken from P3 (see **Figure 3**). The thin sections show parallel-polarized with (a) 10x and (b) 25x magnifications. The C3 is composed of quartz (Qz), feldspar (Fs), bioclast (Fo), calcite (Ca), along micrite (Mc) and sparry calcite (SCa) that fill the spaces between grains.

Bioclast fragments are abundant in lithofacies C2, with average grain sizes ranging from 0.3 mm to 0.18 mm. The bioclasts are primarily composed of foraminiferal skeletal fragments (see **Figure 7a-b, e-f**).

Accessory and silicate minerals are also present in the C2 (see **Figure 7**). The accessory minerals are dominated by glauconite and chlorite. Glauconite grains account for an average of 20.63% of the total framework content and average 0.2 mm in grain size (see **Table 3-4**). The chlorite, however, occurs as detrital monomineralic grains, averaging 3.07% of the total framework and also averaging 0.2 mm in size. These grains commonly interlock with feldspars. Silicate minerals are present in minor amounts, primarily represented by pyroxenes, which average 0.2 mm in grain size (see **Figure 7c–d**).

The matrix and cement are present for an average of 4.8% and 2.1% respectively, showing a ratio of 2 : 1 (see **Table 4**). They are predominantly composed of calcite (see **Figure 7**). The calcite commonly fills interstitial spaces between grains, but also locally replaces bioclast shells, contributing to the diagenetic fabric of the C2 facies.

4.2.2. Petrography of C3

Petrographic analysis of the C3 facies within FA1 was conducted to determine the texture and composition of limestone in the Ombilin Formation (P3; **Figure 3**). The C3 is identified as a poorly sorted, rounded grain, very fine to coarse calcarenite (0.08 to 0.7 mm) limestone, composing of approximately 20% bioclasts, 20% calcite, 10% detrital minerals, 35% micrite, and 15% sparry calcite of cement (see **Figure 8; Table 3-4**). Following **Folk (1959; 1980)** classification, the limestone is classified as intrasparite.

Bioclasts and calcite represent the most abundant components (see **Figure 8**). Although most bioclasts are difficult to identify taxonomically, some are interpreted as debris and skeletal fragments of foraminifera (**c.f. Flugel, 2004**). Calcite commonly appears as a replacement of bioclast material, indicating diagenetic alteration.

Detrital components are primarily represented by monocrystalline quartz of up to 7% and feldspar of up to 3% (see **Figure 8; Table 4**). These grains contribute to the minor clastic input within the limestone. Micrite and sparry calcite, however, are also significant, together comprising half of the rock volume, predominantly filling the spaces between grains, and contributing to the overall fabric and lithification of the C3 facies.

4.2.3. Petrography of S3

Petrographic analysis of the S3 facies within the FA2 was conducted to characterize the texture and composition of non-calcareous sandstones in the Ombilin Formation (P1; **Figure 3**). The S3 is primarily composed of quartz (average of 9.9%), feldspar (average of 57.17%), lithic fragments (average of 14.23%), accessory (average of 9.13%), matrix (average of 3.13%), and cement (average of 6.43%) (see **Figure 9; Table 3-4**). Grain sizes range from 0.2 to 0.6 mm, indicating a fine- to coarse-grained sandstone of **Wentworth's (1922)** classification.

The petrographic analysis revealed that the detrital framework in the S3 is dominated by feldspar, followed by quartz and lithic fragments, each showing diverse morphometric characteristics (see **Figure 9**). Feldspar is characterized by sub-angular to sub-rounded grains, prismatic shapes, and linear contacts with adjacent grains. Quartz is mostly sub-rounded and exhibits linear to convex-concave contacts with one another. Lithic fragments are predominantly volcanic in composition. The volcanic grains are sub-angular to sub-rounded and

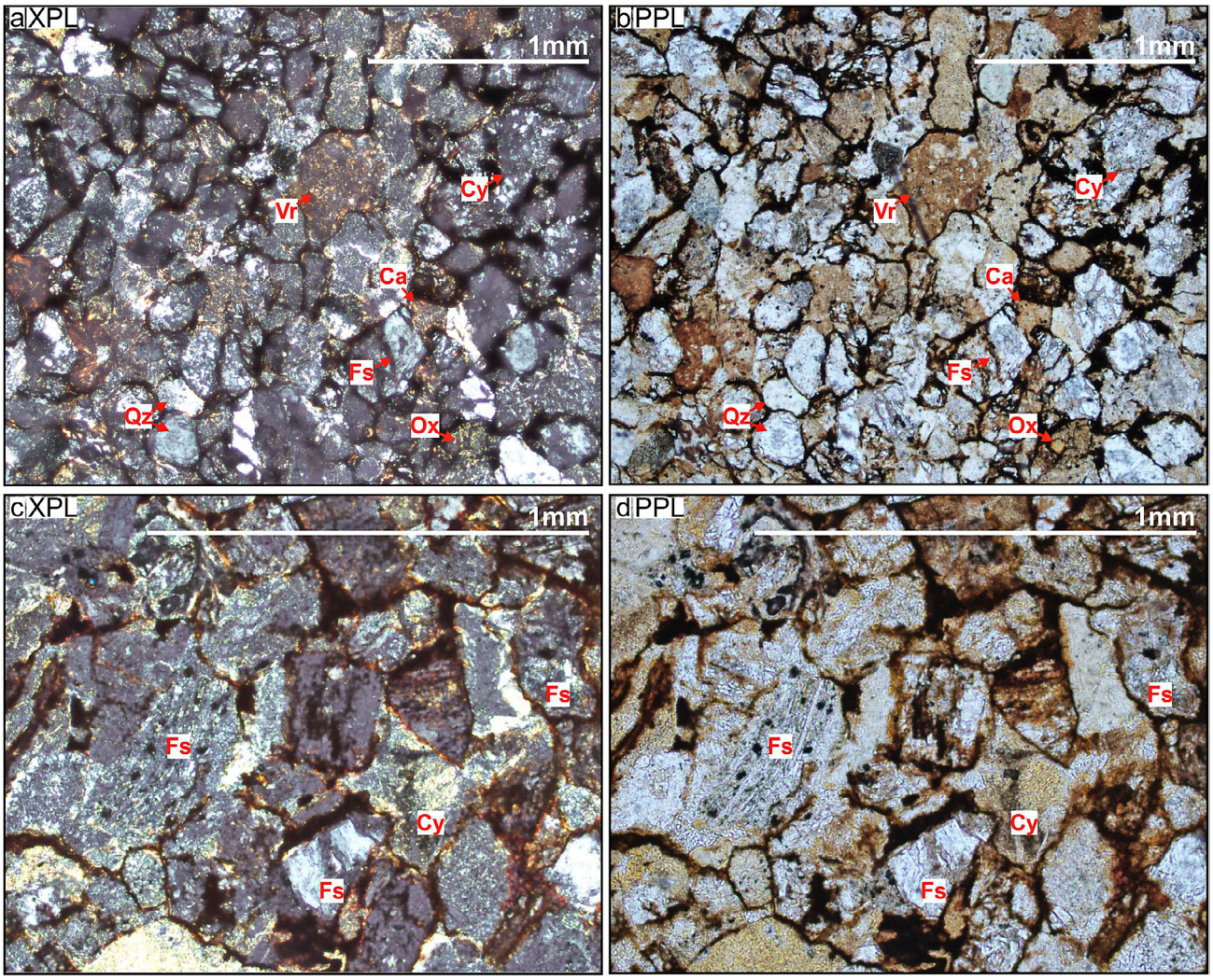

Figure 9. Photomicrographs from thin sections of massive sandstone (S3) of facies association 2 (FA2) in the Ombilin Formation, being taken from P1 (see **Figure 3**). The thin sections show (a) cross- and (b) parallel-polarized with 10x magnifications, and (c) cross- and (d) parallel-polarized with 25x magnifications. The S3 composed of quartz (Qz), feldspar (Fs), volcanic fragments (Vr) and clay (Cy) as matrix, and calcite (Ca) and oxide grains (Ox) as cements.

exhibit linear contacts with neighbouring grains. Normalized point counting was conducted to determine the percentage of QFL framework compositions in the S3. The framework compositions show that the feldspar, quartz, and lithic fragments average 70.87, 11.67, and 17.5% respectively (see **Table 5**). The quartz contains an average of 9% monocrystalline and 2.6% polycrystalline grains.

Accessory minerals include muscovite and opaque minerals (see **Figure 9**). Muscovite occurs with an average of 3.13%, while opaque minerals are present with an average of 6% of the sample. They commonly appear as coatings and stains on quartz grains.

The matrix and cement are present in relatively minor concentrations with an average of 3.13% and 6.43% respectively, showing the ratio of 1 : 2 (see **Figure 9**). The matrix consists of very fine lithic fragments and clay minerals, whereas the cement is mostly composed of very fine calcite, muscovite and oxide minerals. Both components fill pore spaces and occur as coatings on grains, contributing to the overall textural maturity of the S3.

5. Discussions

5.1. Sedimentology of the Ombilin Formation

The three facies that have been described above have been interpreted, indicating three depositional environments. The interpretations are described below.

5.1.1. Sedimentology of FA1: open marine

5.1.1.1. Lithofacies and facies association of FA1

The sedimentary processes and depositional environments of the FA1 have been inferred from the lithological characteristics, petrographic features, and sedimentary structures observed in C1 to C3. The character of lithology in the FA1 consists of calcareous, massive

mudrock (C1), calcareous, ripple-stratified sandstone (C2), and stratified limestone (C3). The C1 and C2 are similarly observed in Sinamar-1, showing calcareous sandstone and calcareous marine-dominated sediments (see **Figure 2; Koning, 1985**).

The fine-grained nature of the calcareous mudrock in the C1 is interpreted in this study as products of suspension setting under low-energy conditions (**e.g. Boggs, 2014; Fakhruddin et al., 2023**), and/or from long-distance horizontal transport of clay aggregates by dynamic processes (**Plint, 2010**). The calcareous composition of these sediments has been attributed to the breakdown of calcareous bioclasts (**Prat, 2010**). Still, the sparry calcite in petrography C3 was formed by precipitation from carbonate solution. Interpretation of the C1 is consistent with previous studies, showing biostratigraphic analysis of the C1 (M1–M3; **Figure 3**), suggesting a littoral marine setting (**Erdi, 2011; Loeblich and Tappan, 1994**), where it was located between high- and low-tide levels (**Hedgpeth, 1957**).

The calcareous ripple-stratified sandstone of the C2 is characterized by the presence of parallel and ripple laminations. These structures have been interpreted as indicators of contrasting flow regimes, with parallel lamination reflecting deposition under upper flow regime conditions, and ripple lamination indicating lower flow regime (**e.g. Simons and Richardson, 1963; Boggs, 2014**). The coexistence of both structures has been attributed to weak and episodic oscillatory currents operating in shallow marine environments (**Pratt, 2010; Longhitano et al., 2021**). Additionally, the occurrence of glauconite within the C2 has been interpreted as a product of early diagenesis, formed under conditions of oxidizing seawater and reducing pore water at depths reaching approximately 60 meters (**e.g. Odin and Matter, 1981; Rubio and Lopez-Perez, 2024**). When considered alongside the fine-grained nature of the sandstone, the presence of glauconite suggests deposition in a lower to middle shoreface setting. This interpretation aligns with analogues of glauconite-bearing very fine sands in shoreface environments, such as those observed along the coast of Rio Grande do Sul (**Plint, 2010**) or Lublin Basin, Poland (**Starzec et al., 2023**).

Within the FA1, the occurrence of the packstone has been identified in the C3. Petrographic observations are suggested for the C3 as intrasparite, that has high in allochemical rock and intraclast compositions, suggesting a shallow depth with sea level fluctuations of calm and high energy environment (**Folk, 1959; 1980**). Given this petrographic observation that suggest sea level fluctuations, this packstone of the C3 has been interpreted as having been deposited on the subtidal part of a carbonate ramp environment. This interpretation is also consistent with analogous occurrences of packstone in Utah, where it is distributed as subtidal cycles within carbonate ramps (**Jones, 2010**), and by Mesozoic packstone successions in Western Newfoundland and Southern Australia, where it is commonly found as a subtidal deposit (**e.g. James and Bone, 1994**; **Pratt, 2010**). The interpretation of the subtidal part of a carbonate ramp environment for the C3 is aligned with biostratigraphic data of the Ombilin Formation in the Sinamar-1 well, located northeast of Section D, which suggests deposition within a sublittoral marine zone (**Koning, 1985; Figures 1 and 2b**).

5.1.1.2 Vertical distributions and interpretation of FA1

The open marine deposits (FA1) are situated beneath the tidally influenced channels (FA2), as evidenced by an erosional contact between the C1 and the S1 (see **Figure 3**). This stratigraphic relationship is further supported by lateral facies changes, with a transition from mud-prone deposits in the central area (Section C) to sand-prone deposits toward the northeast (Section B; **Figure 1b and 3**). These vertical and lateral facies variations reflect a coarsening trend from the FA3 to the FA1 near Tanjung Ampalu (section C; **Figure 3**), indicating a transition from accumulation of suspended-load fines to bedload-dominated transport of tidal-influenced channel in this area. However, from this point northeastward (section B to D), the vertical and lateral facies show an inverse transition, illustrated by the bedload-dominated transport of tidal-influenced channel near Tanjung Ampalu to the accumulation of suspended-load fines in more distal open marine settings northeastward. The observations of normal and inverse transition are aligned with biostratigraphy data of **Erdi (2011)** and **Koning (1985)**, revealing a northeastward shift from littoral in Section C to sublittoral environments in the Sinamar-1 (c.f. **Figures 1b and 2b**). More particularly to the inverse transition, this observation indicates that transgression likely occurred during deposition of the FA1 in section D, which is likely deposited above FA2 and FA3 in section B (see **Figure 3**).

5.1.2. Sedimentology of FA2: tidal influenced channel

5.1.2.1. Lithofacies and facies association of FA2

The sedimentary processes and depositional environments of the FA2 have been interpreted based on lithological characteristics and sedimentary structures identified within facies S1 to S4. The basal conglomerates of the S1 have been interpreted as representing the early stage of channel development (**e.g. Bentham et al., 1993**). Alternatively, the basal conglomerate originated from lag deposits, being associated with thalweg and dune migration (**e.g. Kleinhans et al., 2002; Plink-Bjorklund, 2005; Fakhruddin et al., 2023**). The presence of coal fragments and mud clasts within these conglomerates have been attributed to erosion and transportation of muddy substrates at the channel base (**Li et al., 2017**), with tidal influence inferred from the abundance of mud clasts, consistent with estuarine fluvial settings

(**Dalrymple, 2010**). The amalgamated geometry of the S1 has been interpreted as an indicator of environments that contain a high rate of sedimentary discharge (**e.g. Boggs, 2014**). The occurrence of massive sandstones in the S3, however, have been interpreted as indicators of an environment that contain high depositional rates and rapid deposition (**e.g. Olariu et al., 2010; Olariu and Bhattacharya, 2006; Fakhruddin et al., 2023**). These S1 and S3 facies have been found in environments, such as tidal channels (**e.g. Plink-Bjorklund, 2005; Dalrymple, 2010**), distributary systems (**e.g. Olariu and Bhattacharya, 2006; Gani and Bhattacharya, 2007**), or delta fronts (**e.g. Olariu et al., 2010; Fakhruddin et al., 2023**). Parallel laminations in the S1 and the S2 have been linked to upper flow regime conditions and turbulent sediment transport (**Paola et al., 1989; Boggs, 2014**), possibly representing planar bed flows in lateral accretion sets (**e.g. Plink-Bjorklund, 2005**). Laminated mudrocks and coal stringers in the S1, alongside interbedded sandstone and mudrock in the S2, have been interpreted as rapid accumulation of organic matter near floodplains or in abandoned channels (**cf. Plink-Bjorklund, 2005**). Furthermore, planar cross-stratified sandstones in the S4 have been associated with dune or bar migration, while herringbone cross-stratification in the S4 has been interpreted as evidence for bidirectional currents and 3D dune migration under tidal influence (**Plink-Bjorklund, 2005; Fakhruddin et al., 2023**). Collectively, the presence of (i) basal conglomerates, which indicate early stage and migration of channels, (ii) amalgamated and massive sandstone, which indicates high energy environments, (iii) herringbone cross-stratified sandstones, which indicate bidirectional currents, support the interpretation that the FA2 represents tidally influenced channel deposits.

5.1.2.2. Vertical distributions and interpretation of FA2

The tidal-influenced channels (FA2) have been observed to overlie either mixed tidal flat deposits (FA3) or open marine deposits (FA1; **Figure 3**). The vertical transition from the mixed tidal flats to the tidally influenced channels has been interpreted as evidence for incision of channel systems into previously established intertidal, mixed tidal flat environments. In contrast, transitions from the open marine to the tidal-influenced channel deposits suggest an increase in sediment supply from proximal sources. Erosional surfaces at the base of these channels, particularly where they overlie the open marine deposits, is an indication of progradation of tidal channels into open marine settings.

5.1.3. Sedimentology of FA3: mixed tidal flats

5.1.3.1. Lithofacies and facies association of FA3

The sedimentary processes and depositional environments of the FA3 have been inferred from the lithological characteristics, sedimentary structures, and bioturbation features of S5 to S7. Wavy and flaser stratifications observed in the S5 have been interpreted as products of deposition by reversing tidal currents (**Reineck and Singh, 1980**), indicative of an intertidal setting characterized by diminishing current energy (**Dalrymple, 1992**). Symmetrical rippled laminations in the S6 have been associated with lower flow regimes (**e.g. Simons and Richardson, 1961; Boggs, 2014**), and are considered to have formed during phases of maximum tidal flow (**e.g. Plink-Bjorklund, 2005; Fakhruddin et al., 2023**). These interpretations are supported by the occurrence of *Skolithos linearis* and *Laevicyclus parvus*, which indicate deposition in shallow marine to nearshore environments under tidal influence (**Desjardins et al., 2012; Knaust et al., 2018**). The presence of *Laevicyclus parvus*, an ichnogenus of *Siphonicnus*, has been linked to marginal-marine settings, ranging from proximal offshore and shoreface to estuarine and lagoonal environments, often affected by variable salinity and freshwater influx (**Knaust, 2015; 2018**). Additionally, the rare occurrence of parallel lamination in the S6 has been interpreted as evidence of planar bed flows from traction current (**e.g. Boggs, 2014**; **Plink-Bjorklund, 2005**). In contrast, the massive mudrocks in the S7 are believed to have been deposited from suspension under low-energy conditions (**e.g. Santos and Rossetti, 2006; Fakhruddin et al., 2023**). Collectively, the presence of (i) wavy, flaser, and ripple stratifications, (ii) bioturbation by *Skolithos linearis* and *Laevicyclus parvus*, (iii) thick massive mudrock, and (iv) minor parallel lamination suggest that the FA2 represents intertidal, mixed tidal flat deposits.

5.1.3.2. Vertical distributions and interpretation of FA3

The mixed tidal flat deposits (FA3) are commonly positioned above or interbedded with tidally influenced channel deposits (FA2; **Figure 3**). Vertical transitions from the mixed tidal flats to the tidal channel deposits have been interpreted to reflect incisions of the tidal channel into the underlying mixed tidal flats. Conversely, upward transitions from the tidal channels into the mixed tidal flat deposits indicate lateral migration of the tidal channel over time.

5.2. Sandstone Maturity, Classification and Provenance

The C2 samples have provided insight into sediment maturity, sandstone classification, and provenance related to tectonic settings. Detrital and authigenic minerals exhibit sub-angular to sub-rounded shapes and poor sorting, indicating sub-mature to mature textural characteristics (**cf. Folk, 1980**), and suggesting limited transport from the source. Compositionally, C2 is dominated by feldspar (average of 77.3%) and lithic fragments (average of 21.27%), with minimal to absent quartz content

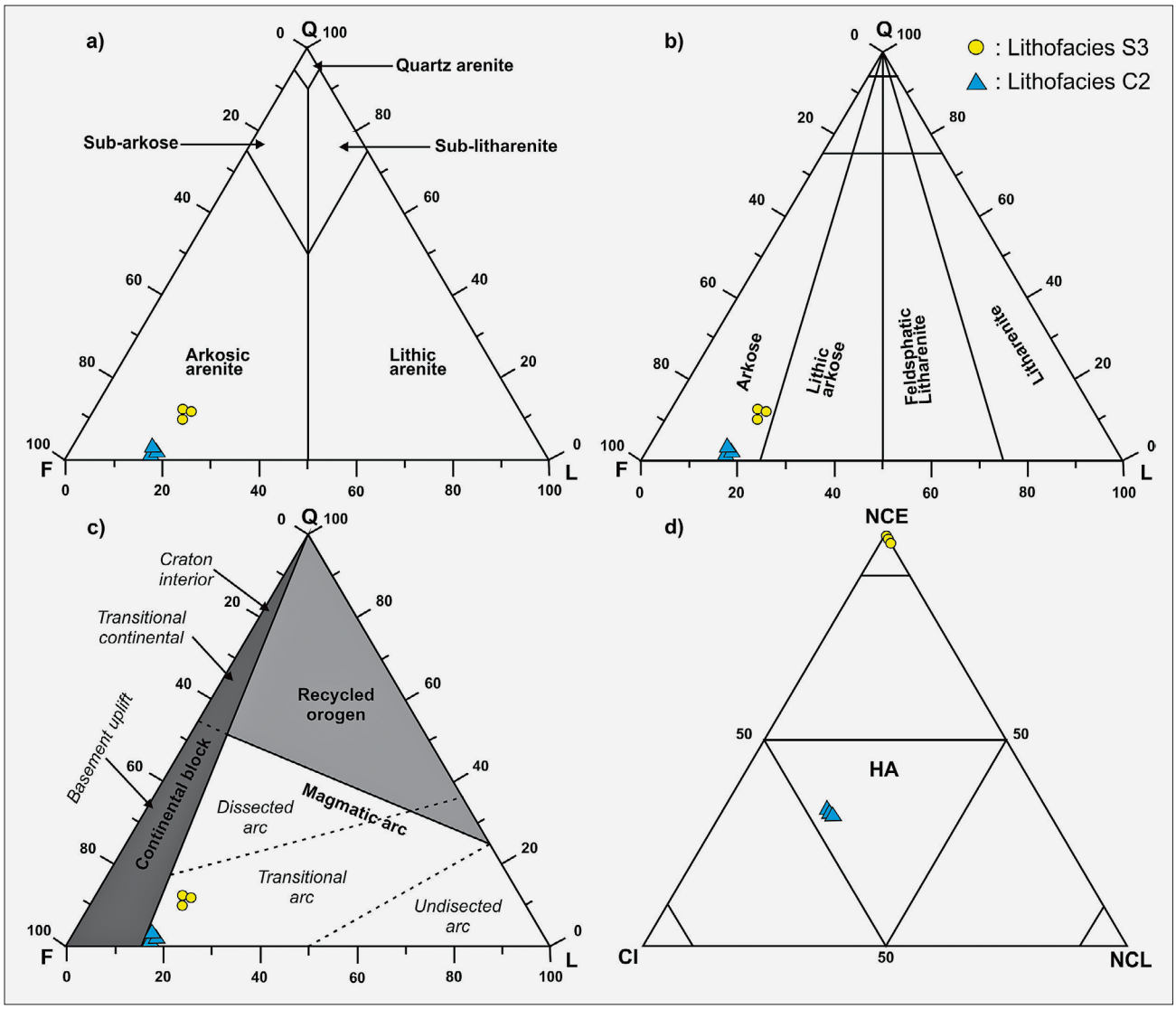

Figure 10. The sandstone composition from the petrography of the Ombilin Formation in the Ombilin Basin based on schemes proposed by (a) **Pettijohn (1975)** and **(b) Folk (1980)**. The sandstone in (a) represents arkosic arenite, while in (b) represents arkose sandstone. (c) The sandstone compositions are plotted on the diagram of **Dickinson et al (1983)** to indicate their provenance. The abbreviations of Q, F, L reflect standard plots of Quartz, Feldspar, and Lithic grains, respectively. (d) Compositions from the petrography are plotted to the schemes proposed by **Zuffa (1980)**. The abbreviation of NCE, CI and NCL reflects non-carbonate extrabasinal, carbonate intrabasinal and intrabasinal non-carbonate respectively in **Table 4**. The HA reflects region of hybrid arenite of **Zuffa (1980)**.

and a ratio of 2:1 for matrix (average of 4.8%) and cement (average of 2.1%) (see **Table 4-5**). These characteristics correspond to arkosic arenite (**Pettijohn, 1975**) or arkose (**Folk, 1980**) classifications (**Figure 10a, b**). Detrital chlorite grains are present, implying the inclusion of chlorite-bearing allogenic lithics derived from metamorphic or igneous sources (**Worden et al., 2020**). Provenance analysis using the **Dickinson et al. (1983)** diagram places the sandstones within the magmatic arc field (see **Figure 10c**), and the high feldspar content supports derivation from intermediate volcanic sources such as andesite (see **Table 4**). Additionally, the high content of bioclast (average of 30.1%) and glauconite (average of 20.63%), which illustrate the high composition of carbonate intrabasinal (CI) and non-carbonate intrabasinal (NCl) respectively, reflecting into the C2 is classified as a hybrid arenite (HA) in the triangular diagram of **Zuffa (1980)** (see **Figure 10d**). Some bioclasts show skeletal fragments, likely suggesting a rework of marine materials. These bioclasts were reported to have been deposited during N4-N5 of the Early Miocene age (**Erdi, 2011**). As such, it is speculated that the marine materials were derived from limestone of the Ombilin Basin, which are distributed along the basin margin (**e.g. Koning, 1985; Anastasia et al., 2012**). Consequently, the provenance of C2 is interpreted as a mixture of volcanic input and reworked marine materials. Such interpretations of a mixture of volcanic input and reworked marine materi-

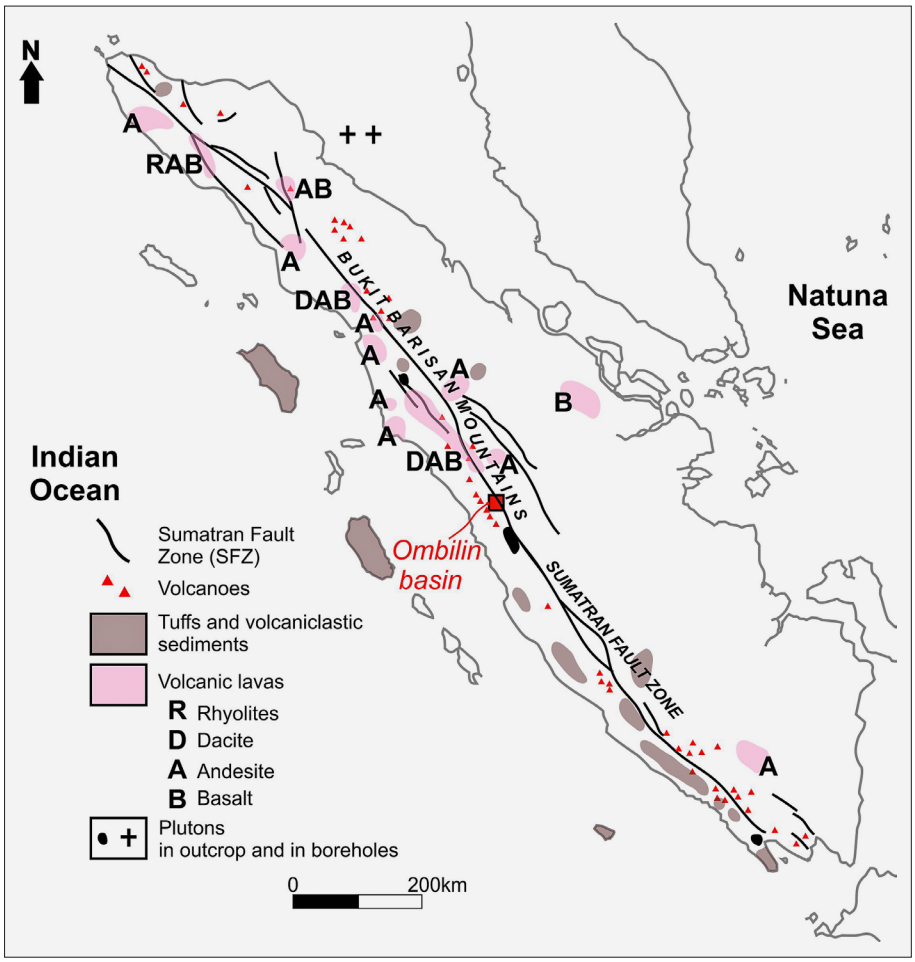

Figure 11. Distributions of Early-Middle Miocene volcanic units in Sumatra (modified from **Barber et al., 2005**). The provenance of the Ombilin Formation is speculated to come from the western part of the basin, where a volcanic chain is present.

als are aligned with earlier studies that link the Ombilin Formation to active volcanism and/or syn-sedimentary reworking (**Adhiperdana, 2010; Yeni, 2011**).

The S3 samples have also revealed information on sediment maturity, sandstone classification, and provenance related to tectonic settings. Detrital and authigenic grains exhibit sub-angular to sub-rounded shapes and poor sorting, indicating a sub-mature to mature texture (**cf. Folk, 1980**), and suggesting limited transport distance from the source. Compositionally, S3 is dominated by feldspar (average of 70.87%), with lower proportions of quartz (average of 11.67%) and lithic fragments (average of 17.5%) (see **Table 5**). Based on these compositions and combined with a ratio of 1:2 for matrix (average of 3.13%) and cement (average of 6.43%) (see **Table 4**), the sandstones have been classified as arkosic arenite (**Pettijohn, 1975**) or arkose (**Folk, 1980**; **Figure 10a, b**). Provenance analysis using the **Dickinson et al. (1983)** diagram places the S3 sandstones within the magmatic arc field (see **Figure 10c**). On the other hand, high non-carbonate extrabasinal (NCE) is shown by the triangular plot of **Zuffa (1980)** (see **Figure 10d**), suggesting extrabasinal origin of high feldspar, moderate lithic fragments, and low quartz, accessory, and heavy mineral content (see **Table 4**). Given the high feldspar content and the tectonic interpretation, the feldspathic assemblages in S3 are inferred to reflect an andesitic source, similar to the result of the C2.

The high feldspar content and a magmatic arc affinity in the S3 and the C2 have been interpreted as consistent with the distribution of Early–Middle Miocene volcanic lavas in Central Sumatra (see **Figure 11**). These volcanic products, predominantly andesitic in composition, were emplaced near the Sumatra Fault Zone and the Barisan Mountains during the emergence and uplift of the Bukit Barisan range in the Early Miocene (**Barber et al., 2005**). The provenance of the Ombilin Formation is therefore inferred to have been derived from volcanic sources situated to the west of the Ombilin Basin (see **Figure 11**). This pattern is similar to observations of provenance for the early syn-rift formations that were deposited during the Eocene in the Ombilin Basin (**Howells, 1997; Barber et al., 2005**).

The Ombilin Formation is underlaid by the Sawahtambang Formation. Several previous studies have illustrated the character of the Sawahtambang Formation. The conglomerate in this formation composed of sedimentary clasts, consisting of volcanic, sedimentary, plutonic and metamorphic fragments (**Howells, 1997**). The distribution of these clasts from this previous study show that

they are characterized by an upward increase in volcanic and sedimentary clast, whereas plutonic and metamorphic clast decrease from bottom to top of the formation. Petrographic analysis of sandstone in the Sawahtambang Formation show characteristic of poor sortation, subangular to sub-rounded grains and non-calcareous (**Erdi, 2011; Putri et al., 2024**). These previous studies show that the Sawahtambang Formation dominantly in quartz, with minor feldspar and sedimentary fragment, reflecting dominantly litharenite and lithic wacke, and minor feldsphatic wacke and arkosic arenite. Previous study has defined that the Sawahtambang Formation is recycled origin, suggesting its origin was related to long process of uplift and erosion (**Putri et al., 2024)**.

The sand-rich sediments in the Ombilin Formation, which is illustrated by the C2 and the S3, has different characteristics compare with the Sawahtambang Formation. Although texture, such as grain sized, sortation and roundness are similar, mineral compositions of the Ombilin Formation show they are relatively higher in feldspar than the Sawahtambang Formation. The presence of lithic fragments and quartz content in C2 and S3 may indicate a rework from underlying formations. We speculate that the Sawahtambang Formation as an origin of this minor mineral content, given that Sawahtambang has high levels of quartz and lithic fragments. As such, the provenance of C2 and S3 is speculatively a mixture of volcanic input, reworked marine materials and clastic materials derived from underlying formations.

5.3. Tectonic Settings and Paleoenvironments in Early-Middle Miocene of the Ombilin Basin

The Ombilin Formation has been defined by several previous studies, occurring as early as the Early Miocene (N4-N5). This formation was deposited during a regional transgression in Sumatra (**Koesoemadinata and Matasak, 1985; Fletcher and Yarmanto, 1993; Situmorang et al., 1991; Barber et al., 2005**), and/or global sea-level rise (**Zaim et al., 2012**). However, the transgression documented in these previous studies are in contradiction to global eustatic events of Mi-1a, Mi-1aa, and Mi-1b glaciation events (**Miller et al., 1998; Morley et al., 2021**). These events are illustrated by Early Miocene Southeast Asia sea-level curves in SEA34–SEA46 (**Morley et al., 2021; Figure 2**). These sea level curve and associated events suggest glacial episodes and associated sea-level falls occurred during the Early Miocene age in SEA34-SEA46, being driven by continental ice-sheet expansion (**Miller et al., 1998; Morley et al., 2021**). Still, global transgression did occur in Early-Middle Miocene, being initiated near SEA52 at the onset of the Middle Miocene Climate Optimum (MMCO) and peaking at SEA53 (**Figure 2; De Boer et al., 2010; Holbourn et al., 2013; Morley et al., 2021).**

The global sea-level fall events in the Early Miocene, during the uplifting of Barisan Mountain in Sumatra, are likely related to the present study that identifies tidal-influenced channels, mixed tidal flat and open marine depositional environment in the Ombilin Formation near Tanjung Ampalu Fault (see **Figure 1b**). The tidal influenced channel (FA2) and mixed tidal flat (FA3) reflect the sub-environment of the estuarine depositional environment near Tanjung Ampalu during the deposition of the Ombilin Formation. Such sub-environments of estuarine origin are also observed in Spitsbergen (**Plink-Bjorklund, 2005; Plink-Bjorklund and Steel, 2006**) and Seven River estuaries (**Dalrymple, 2010**). Such an estuarine depositional environment is also observed during the Early Miocene Bangko Formation in the Central Sumatra Basin, located 17 km northeast from the Ombilin Basin (**e.g. Hendra et al., 2018**). Particularly to the tidal influenced channel, this facies overlies the open marine deposits (FA1), indicating progradation of tidal channels into open marine settings. This observation suggests that regression occurred in the Ombilin Basin. This regression event might result from uplifting, given that isostatic uplifts result in increasing sediment supply and shoreline regressions (**e.g. Catuneanu, 2006; Tsunetaka et al., 2024**). This suggestion is consistent with the Barisan Mountain that underwent uplift in the Early Miocene (**Barber et al., 2005**). Alternatively, this regression might also relate to eustatic sea level fall, given that eustatic sea level fall might destroy accommodation space that induces regression and seaward migration of shoreline (**e.g. Pitman, 1979**; **Catuneanu, 2006**). This suggestion is also consistent with Southeast Asia sea-level curves during the Early Miocene, showing sea-level falls (SEA34–SEA46**; Morley et al., 2021**). As such, this paper suggests that uplifting of Barisan Mountain and sea-level falls occurred, resulting in the deposition of a tidal influenced channel (FA2) and mixed tidal flat (FA3) near Tanjung Ampalu Fault during Early Miocene (see **Figure 12a**). Furthermore, the depositional environment of the tidal-influenced channel and mixed tidal flat in the intertidal, in this study, are consistent with observations of tidal flat facies of calcareous shale and claystone intercalations and *Pelecypods* in Talawi Sub-basin (**Linggadipura et al., 2018**). It was speculated by this study that the Ombilin Formation in the Talawi sub-basin was deposited in the range of supratidal to intertidal environments (see **Figure 12a**). This suggestion is supported by the westward-trending biostratigraphy data, which indicate a landward shift to the west, as reflected by sub-littoral environments in the Sinamar-1 and littoral environment in the section C (**c.f. Koning, 1985** and **Erdi, 2011**).

The calcareous deposits of the Ombilin Formation have been interpreted as neritic to bathyal in origin, based on biostratigraphy data of **Koesoemadinata and Matasak, (1981)** and **Koning (1985**). This study, however, presents the first comprehensive documentation of the presence of tidal-influenced channel sandstones and mixed tidal flat deposits within the Ombilin Formation,

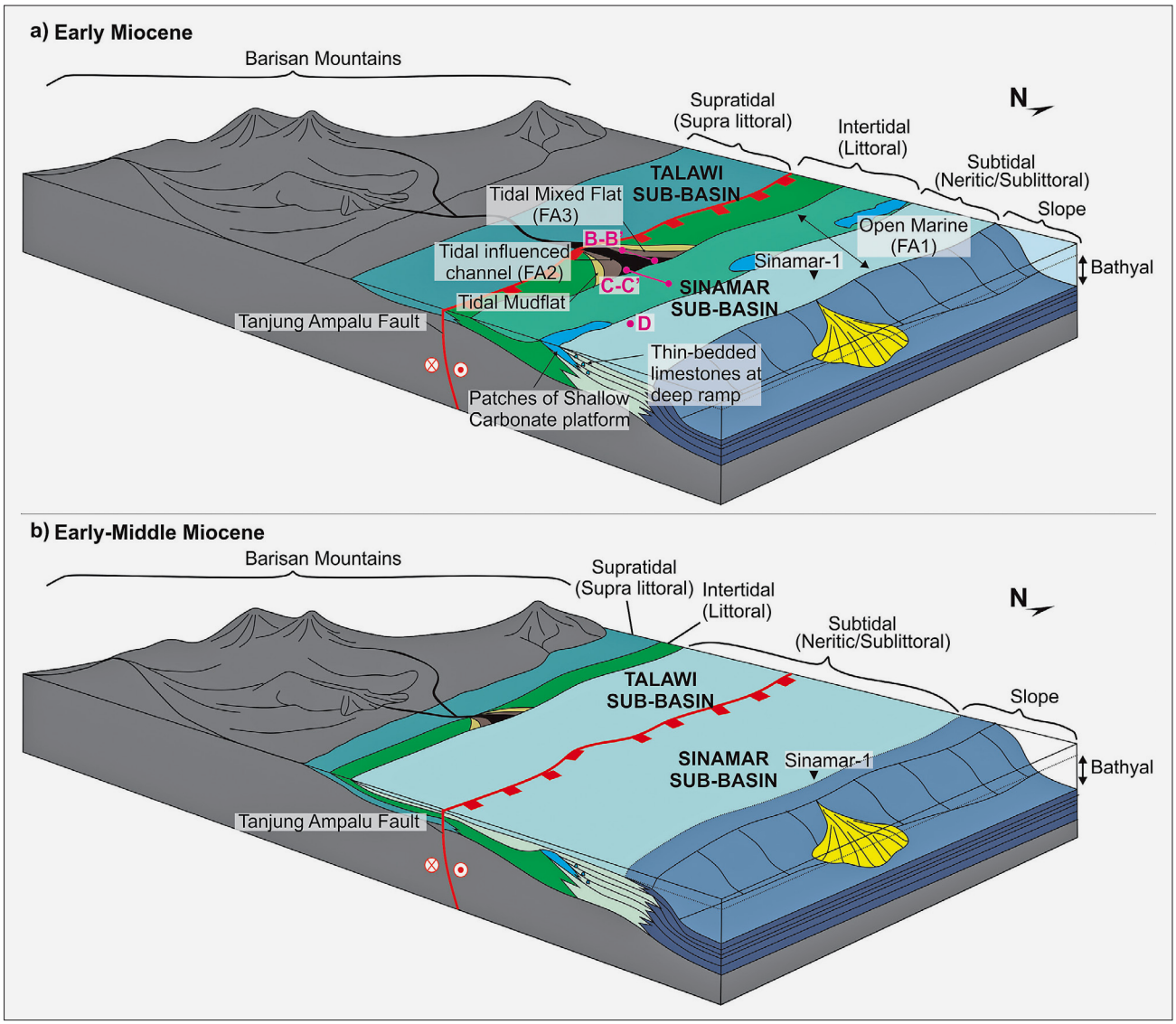

Figure 12. Paleoenvironment of the Ombilin Basin during: (a) Early Miocene, while regional subsidence and eustatic sea level fall occurred in Sumatra and; (b) Early-Middle Miocene, while regional subsidence occurred in Sumatra, eustatic sea level rise due to global transgression (SEA52-54 of **Morley et al., 2021**; **Figure 2**). The black arrow indicates the North (N) direction.

particularly around the basin margins and the Tanjung Ampalu Fault in the Early Miocene. This interpretation is supported by (1) the landward positioning of tidal-influenced deposits relative to calcareous mudrock, (2) the distribution of early limestone facies along basin margins (**Koning, 1985; Anastasia et al., 2012**), (3) increased clastic input attributed to uplift and erosion of the Barisan Mountains (**Barber et al., 2005**), and (4) the long-standing activity of N–S-trending faults such as the Tanjung Ampalu Fault since the mid-Oligocene (**Howells, 1997**). Additionally, volcanism in the western Ombilin Basin during the Early Miocene has been inferred as a major provenance source, despite the absence of direct age dating from these volcanic centres. This interpretation is supported by (1) radiometric dating of andesitic lavas around the Bukit Barisan indicating Early Miocene ages (**Barber et al., 2005; Figure 11**), and (2) the immature to sub-mature texture of Ombilin sandstones, suggesting short transport distances from volcanic sources.

Several previous studies have suggested that the Ombilin Formation continued to be deposited during the Early–Middle Miocene (**Fletcher and Yarmanto, 1993; Howells, 1997**). This event occurred in response to the continuation of a regional transgression in Sumatra (**Koesoemadinata and Matasak, 1985; Fletcher and Yarmanto, 1993; Situmorang et al., 1991; Barber et al., 2005**), and/or global sea-level rise (**Zaim et al., 2012**).

Although comparison between sedimentary log and cross-sections show that section D overlies section B (**c.f. Figure 1b-c** and **3a, c**), this study, however, did not find direct contact between them that indicates certainty of transgression. Nevertheless, based on observation

that the section D overlies section B, where the open marine deposit of FA1 overlie the tidal influenced channel deposits of FA2, this study is suggests that a transgression likely occurred (see **Figure 12b**). It is speculated that the calcareous mudrock of the Ombilin Formation, initially deposited in the deeper parts of the basin, began to accumulate in the study area near the Tanjung Ampalu Fault as a result of global transgression that occurred from SEA 52 to SEA 54 (**Morley et al., 2021**). Additionally, during this period, calcareous mudrocks may have been deposited in the Talawi Sub-basin. The erosional events during the Early–Middle Miocene were driven by ongoing uplift and inversion around the Barisan Mountains (**Barber et al., 2005**). This tectonic activity coincided with the global transgression until SEA 54, followed by regional and global regression extending to the present (**Barber et al., 2005; Morley et al., 2021**).

6. Conclusions

An integrated, detailed analysis of sedimentology and petrography has been provided for the Early-Middle Miocene Ombilin Formation in the Ombilin Basin. Sedimentological analysis of sedimentary logging identified ten lithofacies, being classified into three facies associations: a) open marine deposits (FA1); b) tidal-influenced channels (FA2); and c) intertidal mixed tidal flats (FA3). Their vertical distributions show that FA2-3 are distributed between FA1, reflecting normal and inverse transitions of suspended-load-fines and bedload-dominated transport. The normal transition shows that the FA2-FA3 reflect seaward progradation of tidal channels above open marine settings (FA1). The inverse transition, combined with their spatial distribution along the Tanjung Ampalu Fault, shows that the FA2-3 are likely overlaid by the FA1, speculating a transgression occurred in the Ombilin Basin. Petrographic analysis indicates a submature to mature arkosic composition, derived primarily from a nearby magmatic arc source, with contributions from reworked marine and clastic material derived from the underlying formation(s). The magmatic source is speculated to have originated from Early-Middle Miocene volcanoes located westward of the basin. The evolution of the Ombilin Basin during the Early-Middle Miocene is suggested by the analysis of the sedimentary logging and the petrography, and was influenced by both regional tectonics and global sea-level changes. An initial regression, likely driven by the uplift of Barisan Mountain and global sea level fall, which occurred in the Ombilin Basin during the Early Miocene (SEA34–SEA46). This event was followed by a global transgression that occurred during the Early-Middle Miocene (SEA 52 to SEA 54). This study enhances the understanding of paleoenvironmental evolution and the interplay of tectonic and sea-level controls on sedimentation not only in the intermontane setting of the Ombilin Basin, but also the Sumatra and South East Asia during the Early-Middle Miocene.

Acknowledgement

Some data in this paper is part of the bachelor thesis of the first authors, being supervised by the fourth author. The thesis was conducted in 2011, being sponsored by PT Radiant Bukit Barisan (now PT. Rizki Bukit Barisan Energi). As such, we wish to say thank you to the management of PT Radiant Bukit Barisan, especially to Litto Habrianta Tarigan. We also wish to thank all staff and students in Institut Teknologi Bandung for all their effort and cooperation.

7. References

Adhiperdana, B. G. (2010). A Preliminary Account Of The Framework Grain Composition And Provenance Of The Lower Tertiary Sandstone Outcropped In The Ombilin Basin, Central Sumatra. Bulletin of Scientific Contribution, 8(3), 141-157. https://doi.org/ https://doi.org/10.24198/bsc.v8i3.8252

Anastasia, S., Sitanggang, B. P., Lie, H. S., & Syafri, I. (2012). Ombilin Basin: A Prospect for Shale Gas In Indonesia. Proceedings Indonesia Petroleum Association, the 36th Annual Convention & Exhibition, Jakarta.

Anderton, R. (1985). Clastic facies models and facies analysis. Geological Society, London, Special Publications, 18(1), 31-47. https://doi.org/10.1144/GSL.SP.1985.018.01.03

Augustsson, C. (2021). Influencing Factors on Petrography Interpretations in Provenance Research – A Case-Study Review. Geosciences, 11(5).

Barber, A. J., Crow, M. J., & Milsom, J. S. (2005). Sumatra: Geology, Resources and Tectonic Evolution (Vol. 31). Geological Society, London.

Bartram, K. M., & Nugrahaningsih, L. (1990). A palynological study of the Sawahlunto Formation, Ombilin Basin, West Sumatra. Scientific Contributions/90 Special Issue.

Bentham, P. A., Talling, P. J., & Burbank, D. W. (1993). Braided stream and flood-plain deposition in a rapidly aggrading basin: the Escanilla formation, Spanish Pyrenees. Geological Society, London, Special Publications, 75(1), 177-194. https://doi.org/10.1144/GSL.SP.1993.075.01.11

Boggs, S. (2014). Principles of Sedimentology and Stratigraphy Pearson Education Limited.

Catuneanu, O. (2006). Principles of Sequence Stratigraphy. Elsevier, Amsterdam.

Dalrymple, R. W. (1992). Tidal depositional systems. In R. G. Walker & N. P. James (Eds.), Facies Model: Response to Sea Level Change (pp. 195-218). Geological Association of Canada.

Dalrymple, R. W. (2010). Tidal depositional systems. In N. P. James & R. W. Dalrympe (Eds.), Facies Model 4 (pp. 201-231). Geological Association of Canada.

De Boer, B., van de Wal, R. S. W., Bintanja, R., Lourens, L. J., & Tuenter, E. (2010). Cenozoic global ice-volume and temperature simulations with 1-D ice-sheet models forced by benthic δ18O records. Annals of Glaciology, 51(55), 23-33. https://doi.org/10.3189/172756410791392736

Desjardins, P. R., Buatois, L. A., Pratt, B. R., & MÁNgano, M. G. (2012). Sedimentological–ichnological model for tide-

dominated shelf sandbodies: Lower Cambrian Gog Group of western Canada. Sedimentology, 59(5), 1452-1477. https://doi.org/10.1111/j.1365-3091.2011.01312.x

Dickinson, W. R. (1985). Interpreting Provenance Relations from Detrital Modes of Sandstones. In G. G. Zuffa (Ed.), Provenance of Arenites (pp. 333-361). Springer Netherlands. https://doi.org/10.1007/978-94-017-2809-6_15

Dickinson, W. R., Beard, L. S., Brakenridge, G. R., Erjavec, J. L., Ferguson, R. C., Inman, K. F., Knepp, R. A., Lindberg, F. A., & Ryberg, P. T. (1983). Provenance of North American Phanerozoic sandstones in relation to tectonic setting. GSA Bulletin, 94(2), 222-235. https://doi.org/10.1130/0016-7606(1983)94<222:PONAPS>2.0.CO;2

Erdi, A. (2011). Geologi Daerah Bukitbual Dan Sekitarnya, Kabupaten Sijunjung, Provinsi Sumatera Barat [Institut Teknologi Bandung]]. Bandung.

Erdi, A., Setiawan, A., Zulmi, I., Inabuy, A. R., Zahra, R. H., Edwin, E., Andhika, I. P., Auliansyah, D., & E., W. (2025). Middle-Late Miocene Tidal-related Deposits of the Binio Formation: the Sedimentary and Stratigraphic Records during Inversion of the Central Sumatra Basin, Indonesia. Rudarsko-geološko-naftni zbornik, 40(1). https://doi.org/10.17794/rgn.2025.1.10

Fakhruddin, R., Sunardi, E., Adhiperdana, B. G., Zajuli, M. H. H., Ramli, T., Saleh, H. M., Putra, A. P., Sabra, E., & Arvyalin, G. G. (2023). Late Miocene to Pliocene delta-lacustrine to incised-valley fills sedimentation of the Ransiki Area, Bird's Head Papua, Indonesia: The sedimentary record of Lengguru Fold and Thrust Belt wedge-top depozone. Journal of Asian Earth Sciences, 242, 105497. https://doi.org/10.1016/j.jseaes.2022.105497

Fletcher, G., & Yarmanto. (1993). Post Convention Field Trip: Ombilin Basin Field Guide Book. Indonesian Petroleum Association.

Flügel, E. (2004). Microfacies of Carbonate Rocks. Springer, New York. https://doi.org/10.1007/978-3-662-08726-8

Folk, R. L. (1959). Practical Petrographic Classification of Limestones. AAPG Bulletin, 43(1), 1-38. https://doi.org/10.1306/0BDA5C36-16BD-11D7-8645000102C1865D

Folk, R. L. (1980). Petrology of Sedimentary Rocks. Hemphill Publishing Company, Texas.

Gani, M. R., & Bhattacharya, J. P. (2007). Basic Building Blocks and Process Variability of a Cretaceous Delta: Internal Facies Architecture Reveals a More Dynamic Interaction of River, Wave, and Tidal Processes Than Is Indicated by External Shape. Journal of Sedimentary Research, 77(4), 284-302. https://doi.org/10.2110/jsr.2007.023

Habrianta, L., Matthew, G., Fakhrurozi, F., Auliansyah, D., & Andhika, I. P. (2018). A Semi-Regional Play Analysis Of The Ombilin Basin To Understand The Tectono-Stratigraphic Framework And Identification Of Potential Exploration Opportunities. Proceedings Indonesian Petroleum Association, the 42nd Annual Convention & Exhibition, Jakarta.

Hedgpeth, J. W. (1957). Chapter 2: Classification of Marine Environments*. In J. W. Hedgpeth (Ed.), Treatise on Marine Ecology and Paleoecology (pp. 0). Geological Society of America. https://doi.org/10.1130/MEM67V1-p17

Hendra, H., Wulandari, R., Regina, A., Meilany, H., Gunawan, I. M., Hayatulah, M. S., Thamrin, M. H., Zainal, A. F., & Raihan. (2018). Bangko Shaly Sand Is The Key For The Future To Be Main Reservoir And Increase Oil Production With The Fracturing Stimulation In Beruk Field, Coastal Plan Pekanbaru Block, Central Sumatra Basin. Prosiding Simposium Ikatan Ahli Teknik Perminyakan Indonesia (IATMI) 2018, Padang.

Holbourn, A., Kuhnt, W., Frank, M., & Haley, B. A. (2013). Changes in Pacific Ocean circulation following the Miocene onset of permanent Antarctic ice cover. Earth and Planetary Science Letters, 365, 38-50. https://doi.org/https://doi.org/10.1016/j.epsl.2013.01.020

Howells, C. (1997). Tertiary response to oblique subduction and indentation in Sumatra, Indonesia: new ideas for hydrocarbon exploration. Geological Society, London, Special Publications, 126(1), 365-374. https://doi.org/10.1144/GSL.SP.1997.126.01.22

Irwansyah, Kurniadi, D., Habrianta, L., Reza, T., & Yogi, A. (2018). High Resolution Biostratigraphy And Correlation Accross Paleogene Boundaries In The Ombilin Basin, West Sumatra. Simposium Ikatan Ahli Teknik Perminyakan Indonesia 2018, Padang.

James, N. P., & Bone, Y. (1994). Paleoecology of Cool-Water, Subtidal Cycles in Mid-Cenozoic Limestones, Eucla Platform, Southern Australia. PALAIOS, 9(5), 457-476. https://doi.org/10.2307/3515136

Jones, B. (2010). Warm-Water Neritic Carbonates. In N. P. James & R. W. Dalrympe (Eds.), Facies Model 4 (pp. 341-370). Geological Association of Canada.

Katili, J. A., & Hehuwat, F. (1967). On the occurrence of large transcurrent faults in Indonesia. Journal of Geosciencese, 10, 5-16.

Kleinhans, M. G., Wilbers, A. W. E., De Swaaf, A., & Van Den Berg, J. H. (2002). Sediment Supply-Limited Bedforms in Sand-Gravel Bed Rivers. Journal of Sedimentary Research, 72(5), 629-640. https://doi.org/10.1306/030702720629

Knaust, D. (2015). Siphonichnidae (new ichnofamily) attributed to the burrowing activity of bivalves: Ichnotaxonomy, behaviour and palaeoenvironmental implications. Earth-Science Reviews, 150, 497-519. https://doi.org/10.1016/j.earscirev.2015.07.014

Knaust, D., Thomas, R. D. K., & Curran, H. A. (2018). Skolithos linearis Haldeman, 1840 at its early Cambrian type locality, Chickies Rock, Pennsylvania: Analysis and designation of a neotype. Earth-Science Reviews, 185, 15-31. https://doi.org/10.1016/j.earscirev.2018.05.009

Koesoemadinata, R. P. (2020). Geology of Indonesia Vol I: General Introduction and Part I Western Indonesia (Vol. 1). Ikatan Alumni Teknik Geologi ITB.

Koesoemadinata, R. P., & Matasak, T. (1981). Stratigraphy and sedimentation – Ombilin basin, Central Sumatra (West Sumatra Province). Proceedings Indonesian Petroleum Association, the 10th Annual Convention & Exhibition, Jakarta.

Koning, T. (1985). Petroleum geology of the Ombilin intermontane basin, West Sumatra. Proceedings Indonesian Petroleum Association, the 14th Annual Convention Jakarta.

Li, S., Shan, X., Gong, C., & Yu, X. (2017). Classification, formation, and transport mechanisms of mud clasts. International Geology Review, 59(12), 1609-1620. https://doi.org/10.1080/00206814.2017.1287014

Linggadipura, R. D., Fernando, R. E., Prasetyo, M. H., Krestanu, A., Addiansyah, M., & Susilo, B. K. (2018). Architectural, Facies, And Depositional Environment Analysis Of Paleogene To Neogene Deposit In The Northern Ombilin Basin: Implication Hydrocarbon Potential. Retrieved 2025 from https://geosriwijaya.com/wp-content/uploads/2017/11/Linggadipura-et-al-2018-Architectural-Facies-and-Depositional-Environment-Analysis-of-Paleogene-to-Neogene-Deposit.pdf

Loeblich, A. R., Jr., & Tappan, H. (1994). Foraminifera Of The Sahul Shelf And Timor Sea. In A. R. Loeblich, Jr. & H. Tappan (Eds.), Foraminifera of the Sahul Shelf and Timor Sea (Vol. 31, pp. 0). Cushman Foundation for Foraminiferal Research.

Longhitano, S. G., Rossi, V. M., Chiarella, D., Mellere, D., Tropeano, M., Dalrymple, R. W., Steel, R. J., Nappi, A., & Olita, F. (2021). Anatomy of a mixed bioclastic–siliciclastic regressive tidal sand ridge: Facies-based case study from the lower Pleistocene Siderno Strait, southern Italy. Sedimentology, 68(6), 2293-2333. https://doi.org/https://doi.org/10.1111/sed.12853

Longley Ian, M. (1997). The tectonostratigraphic evolution of SE Asia. Geological Society, London, Special Publications, 126(1), 311-339. https://doi.org/10.1144/GSL.SP.1997.126.01.19

MacEachern, J. A., Pemberton, S. G., Gingras, M. K., & Bann, K. L. (2010). Ichnology and Facies Models. In N. P. James & R. W. Dalrympe (Eds.), Facies Model 4 (pp. 19-58). Geological Association of Canada.

Malaza, N., Liu, K., & Zhao, B. (2016). Petrology and geochemistry of clastic sedimentary rocks as evidences for provenance of the Late Palaeozoic Madzaringwe Formation, Tshipise-Pafuri Basin, South Africa. Science China Earth Sciences, 59(12), 2411-2426. https://doi.org/10.1007/s11430-016-5274-z

Miller, K. G., Mountain, G. S., Browning, J. V., Kominz, M., Sugarman, P. J., Christie-Blick, N., Katz, M. E., & Wright, J. D. (1998). Cenozoic global sea level, sequences, and the New Jersey Transect: Results From coastal plain and continental slope drilling. Reviews of Geophysics, 36(4), 569-601. https://doi.org/https://doi.org/10.1029/98RG01624

Morley, R. J., Hasan, S. S., Morley, H. P., Jais, J. H. M., Mansor, A., Aripin, M. R., Nordin, M. H., & Rohaizar, M. H. (2021). Sequence biostratigraphic framework for the Oligocene to Pliocene of Malaysia: High-frequency depositional cycles driven by polar glaciation. Palaeogeography, Palaeoclimatology, Palaeoecology, 561. https://doi.org/10.1016/j.palaeo.2020.110058

Moss, S. J., & Carter, A. (1996). Thermal histories of Tertiary sediments in western central Sumatra, Indonesia. Journal of Southeast Asian Earth Sciences, 14(5), 351-371. https://doi.org/https://doi.org/10.1016/S0743-9547(96)00071-2

Murray, A. M. (2020). Early Cenozoic Cyprinoids (Ostariophysi: Cypriniformes: Cyprinidae and Danionidae) from Sumatra, Indonesia. Journal of Vertebrate Paleontology, 40(1), e1762627. https://doi.org/10.1080/02724634.2020.1762627

Noeradi, D., Djuhaeni, & Simanjuntak, B. (2005). Rift play in Ombilin basin outcrop, West Sumatra. Proceedings Indonesian Petroleum Association, the 30th Annual Convention, Jakarta.

Odin, G. S., & Matter, A. (1981). De glauconiarum origine. Sedimentology, 28(5), 611-641. https://doi.org/https://doi.org/10.1111/j.1365-3091.1981.tb01925.x

Olariu, C., & Bhattacharya, J. P. (2006). Terminal Distributary Channels and Delta Front Architecture of River-Dominated Delta Systems. Journal of Sedimentary Research, 76(2), 212-233. https://doi.org/10.2110/jsr.2006.026

Olariu, C., Steel, R. J., & Petter, A. L. (2010). Delta-front hyperpycnal bed geometry and implications for reservoir modeling: Cretaceous Panther Tongue delta, Book Cliffs, Utah. AAPG Bulletin, 94(6), 819-845. https://doi.org/10.1306/11020909072

Paola, C., Wiele, S. M., & Reinhart, M. A. (1989). Upper-regime parallel lamination as the result of turbulent sediment transport and low-amplitude bed forms. Sedimentology, 36(1), 47-59. https://doi.org/https://doi.org/10.1111/j.1365-3091.1989.tb00819.x

Pettijohn, F. J. (1975). Sedimentary Rocks (Third Edition ed.). Harper and Row, New York.

Pitman, W. C., III. (1979). The Effect of Eustatic Sea Level Changes on Stratigraphic Sequences at Atlantic Margins1. In Geological and Geophysical Investigations of Continental Margins (Vol. 29, pp. 0). American Association of Petroleum Geologists. https://doi.org/10.1306/M29405C30

Plink-BjÖRklund, P. (2005). Stacked fluvial and tide-dominated estuarine deposits in high-frequency (fourth-order) sequences of the Eocene Central Basin, Spitsbergen. Sedimentology, 52(2), 391-428. https://doi.org/https://doi.org/10.1111/j.1365-3091.2005.00703.x

Plint, A. G. (2010). Wave- and Strom-Dominated Shoreline and Shallo-Marine Systems. In N. P. James & R. W. Dalrympe (Eds.), Facies Model 4 (pp. 167-200). Geological Association of Canada.

Pratt, B. R. (2010). Peritidal Carbonate. In N. P. James & R. W. Dalrympe (Eds.), Facies Model 4 (pp. 401-420). Geological Association of Canada.

Putra, A. F., Abdullah, C. I., & Noeradi, D. (2021). Ombilin Basin as Inverted Oblique Rift in Barisan Mountains, Sumatra: Considerations on Subsidence Mechanisms and Fault Development. IAGI Journal.

Reineck, H. E., & Singh, l. B. (1980). Depositional Sedimentary Environments. Springer-Verlag, Berlin.

Rubio, B., & López-Pérez, A. E. (2024). Exploring the genesis of glaucony and verdine facies for paleoenvironmental interpretation: A review. Sedimentary Geology, 461, 106579. https://doi.org/https://doi.org/10.1016/j.sedgeo.2024.106579

Santos, A. E. A., & Rossetti, D. F. (2006). Depositional model of the Ipixuna formation (Late Cretaceous- Early Tertiary), Rio Capim area, northern Brazil. Latin Am. J. Sedimentol. Basin Analysis, 13.

Simons, D. B., & Richardson, E. V. (1963). Forms of Bed Roughness in Alluvial Channels. Transactions of the

American Society of Civil Engineers, 128(1), 284-302. https://doi.org/10.1061/TACEAT.0008730

Situmorang, B., Yulihanto, B., Guntur, A., Himawan, R., & Jacob, T. G. (1991). Structural Development of the Ombilin Basin West Sumatra. Proceedings Indonesian Petroleum Association, the 20th Annual Convention, Jakarta.

Starzec, K., Stadnik, R., Skiba, M., Bębenek, S., & Waśkowska, A. (2023). Origin and paleoenvironmental significance of Al-rich glauconite in the Ediacaran/Cambrian deposits of the Lublin Basin, Poland (SW margin of Baltica). Precambrian Research, 397, 107165. https://doi.org/https://doi.org/10.1016/j.precamres.2023.107165

Tsunetaka, H., Murakami, W., & Daimaru, H. (2024). Shoreline advance due to the 2024 Noto Peninsula earthquake. Scientific Reports, 14(1), 28026. https://doi.org/10.1038/s41598-024-79044-4

Van Bemmelen, R. W. (1949). General Geology of Indonesia and Adjacent Archipelagoes (Vol. I). Goverment Printing Office, The Hague.

Wentworth, C. K. (1922). A Scale of Grade and Class Terms for Clastic Sediments. The Journal of Geology, 30(5), 377-392. https://doi.org/10.1086/622910

Whateley, M. K. G., & Jordan, G. R. (1989). Fan-delta-lacustrine sedimentation and coal development in the Tertiary Ombilin Basin, W Sumatra, Indonesia. Geological Society, London, Special Publications, 41(1), 317-332. https://doi.org/10.1144/GSL.SP.1989.041.01.22

Worden, R. H., Griffiths, J., Wooldridge, L. J., Utley, J. E. P., Lawan, A. Y., Muhammed, D. D., Simon, N., & Armitage, P. J. (2020). Chlorite in sandstones. Earth-Science Reviews, 204, 103105. https://doi.org/https://doi.org/10.1016/j.earscirev.2020.103105

Yeni, Y. F. (2011). Perkembangan Sedimentasi Formasi Brani, Formasi Sawahlunto Dan Formasi Ombilin Ditinjau Dari Provenance Dan Komposisi Batupasir Cekungan Ombilin Proceedings JCM Makassar 2011, The 36th HAGI and 40th IAGI Annual Convention and Exhibition, Makassar.

Zaim, Y., Habrianta, L., Abdullah, C. I., Aswan, Rizal, Y., Basuki, N. I., & Sitorus, F. E. (2012). Depositional History and Petroleum Potential of Ombilin Basin, West Sumatra - Indonesia, Based on Surface Geological Data. AAPG International Convention and Exhibition, Singapore.

Zakaria, A. A., Johnson, H. D., Jackson, C. A. L., & Tongkul, F. (2013). Sedimentary facies analysis and depositional model of the Palaeogene West Crocker submarine fan system, NW Borneo. Journal of Asian Earth Sciences, 76, 283-300. https://doi.org/https://doi.org/10.1016/j.jseaes.2013.05.002

SAŽETAK

Organizacija facijesa i podrijetlo sedimenata miocenske formacije Ombilin: međudjelovanje tektonike i eustazije u neogenskome unutarplaninskom bazenu, Središnja Sumatra, Indonezija

Ranomiocenska ombilinska formacija u unutarplaninskome Ombilinskom bazenu, Središnja Sumatra, bilježi ključni interval paleoekoloških promjena uzrokovanih regionalnom tektonikom i globalnim fluktuacijama razine mora. Unatoč važnosti, raspored facijesa sedimentnih stijena, podrijetlo sedimenta i povijest oscilacija razine mora ove formacije slabo su istraženi. Ova studija integrira detaljno sedimentološko istraživanje i petrografsku analizu izdanaka s ciljem dobivanja novih spoznaja o navedenim nedostatcima. Identificirano je deset litofacijesa koji su grupirani u tri asocijacije facijesa: facijes otvorenoga mora, facijes plimnih kanala i facijes međuplimne zone s plimnom ravnicom. Njihov vertikalni raspored upućuje na postojanje normalnih i inverznih prijelaza. Normalni prijelaz upućuje na pomak od sublitoralnih do plimom dominiranih okoliša, što se tumači kao rezultat povećanoga donosa sedimenta s uzdignutih planina Barisan te kratkoročnim globalnim padom razine mora (npr. SEA34–SEA46). S druge strane, inverzni prijelaz upućuje na transgresiju koja se dogodila u Ombilinskome bazenu. Petrografska analiza u formaciji Ombilin uputila je na postojanje arkoznih pješčenjaka koji potječu ponajprije iz magmatskoga luka, što je u skladu s istovremenim vulkanizmom koji se odvija zapadno od promatranoga bazena, ali s manjom preradom marinskih naslaga i starijih klastičnih naslaga. Stratigrafski dokazi upućuju na početnu regresiju, vjerojatno uzrokovanu podizanjem planine Barisan i globalnim padom razine mora u bazenu Ombilin tijekom ranoga miocena. Nakon ovoga događaja uslijedilo je taloženje praćeno globalnim transgresivnim trendovima. Ovi nalazi pružaju nove znanstvene spoznaje o razvoju sedimentacije, podrijetlu i tektonsko-eustatičkoj interakciji koja je kontrolirala razvoj bazena Ombilin tijekom ranoga i srednjega miocena.

Ključne riječi:
naslage povezane s plimom, podbazen Sinamar, sedimentologija, podrijetlo, tektonika

Author's contribution

Aurio Erdi (PhD): conceptualization, data curation, formal analysis, methodology, project administration, resources, validation, visualization, writing – original draft, and writing – review and editing. **Syahreza Saidina Angkasa** (PhD): formal analysis, investigation, methodology, and writing – review and editing. **Eko Suwarno** (M. Sc): data curation, and writing – review and editing. **Aswan** (PhD): supervision, validation, and writing – review and editing.
All authors have read and agreed to the published version of the manuscript.